Available online at www.sciencedirect.com
ScienceDirect
Geochimica et Cosmochimica Acta 70 (2006) 4196–4214
Geochimica
www.elsevier.com/locate/gca

Antimony speciation in saline hydrothermal fluids: A combined X-ray absorption fine structure spectroscopy and solubility study

Gleb S. Pokrovski [a,*], Anastassia Yu. Borisova [a], Jacques Roux [b], Jean-Louis Hazemann [c], Alain Petdang [a], Marie Tella [a], Denis Testemale [c]

[a] *Experimental Geochemistry and Biogeochemistry Group, LMTG, UMR 5563, CNRS-OMP-Université Paul-Sabatier, 14 Avenue Edouard Belin, 31400 Toulouse, France*
[b] *IPGP-CNRS, UMR 7047, 4 Place Jussieu, 75252 Paris, Cedex 05, France*
[c] *Laboratoire de Cristallographie-CNRS-SNBL/ESRF, 6 rue Jules Horrowitz, B.P. 220, 38043 Grenoble, France*

Received 6 March 2006; accepted in revised form 16 June 2006

Abstract

Solubility of senarmontite (Sb_2O_3, cubic) in pure water and NaCl–HCl aqueous solutions, and local atomic structure around antimony in these fluids were characterized using in situ X-ray absorption fine structure (XAFS) spectroscopy at temperatures to 450 °C and pressures to 600 bars. These experiments were performed using a new X-ray cell which allows simultaneous measurement of the absolute concentration of the absorbing element in the fluid, and atomic environment around the absorber. Results show that aqueous Sb(III) speciation is dominated by the $Sb(OH)_3^\circ$ complex in pure water, mixed Sb-hydroxide-chloride complexes in acidic NaCl–HCl solutions (2 m NaCl–0.1 m HCl), and by Sb-chloride species in concentrated HCl solutions (3.5 m HCl). Interatomic Sb–O and Sb–Cl distances in these complexes range from 1.96 to 1.97 Å and from 2.37 to 2.47 Å, respectively. These structural data, together with senarmontite solubility determined from XAFS spectra, were complemented by batch-reactor measurements of senarmontite and stibnite (Sb_2S_3, rhombic) solubilities over a wide range of HCl and NaCl concentrations from 300 to 400 °C. Analysis of the whole dataset shows that Sb(III) speciation in high-temperature moderately acid ($pH > 2$–3) Cl-rich fluids is dominated by mixed hydroxy-chloride species like $Sb(OH)_2Cl^\circ$ and $Sb(OH)_3Cl^-$, but other species containing two or three Cl atoms appear at higher acidities and moderate temperatures ($\leqslant$300 °C). Calculations using stability constants retrieved in this study indicate that mixed hydroxy-chloride complexes control antimony transport in saline high-temperature ore fluids at acidic conditions. Such species allow for a more effective Sb partitioning into the vapor phase during boiling and vapor–brine separation processes occurring in magmatic-hydrothermal systems. Antimony hydroxy-chloride complexes are however minor in the neutral low- to moderate-temperature solutions ($\leqslant$250–300 °C) typical of Sb deposits formation; the antimony speciation in these systems is dominated by $Sb(OH)_3$ and potentially Sb-sulfide species.

1. Introduction

This study is aimed at better quantifying the identity, stability and structure of antimony (Sb) aqueous complexes responsible for the transport of this element by high-temperature geological fluids. Although antimony is a trace element on the Earth, with an average continental crust abundance of 0.2 part per million (ppm) and typical concentrations of less than 0.001 ppm in non-polluted surficial waters (e.g., Filella et al., 2002; Rudnick and Gao, 2003; references therein), this element is easily mobilized by high-temperature hydrothermal fluids, attaining concentrations of tens to hundreds ppm as inferred from analyses of fluid inclusions and modern hydrothermal sources (e.g., Audédat et al., 2000; Simmons and Browne, 2000). This fluid enrichment, also typical for other chemically similar metalloids (e.g., As, Ge and Se), renders antimony an important constituent of hydrothermal–volcanic ore deposits. In hydrothermal environments, Sb forms its own sulfide minerals such as stibnite (Sb_2S_3) and numerous Cu–Ag–Pb–As sulfosalts, or enters as a minor component into

* Corresponding author. Fax: +33 0 5 61 33 25 60.
E-mail address: pokrovsk@lmtg.obs-mip.fr (G.S. Pokrovski).

0016-7037/$ - see front matter © 2006 Elsevier Inc. All rights reserved.
doi:10.1016/j.gca.2006.06.1549

arsenopyrite, galena, pyrite, chalcopyrite or sphalerite at levels up to several percent (e.g., Boyle and Jonasson, 1984; Abraitis et al., 2004). The most interesting feature of Sb hydrothermal behavior is its close association with precious and technologically important metals like Au, Ag, W, Pt, Pd and U in many types of mineral deposits (e.g., Boyle and Jonasson, 1984; Mernagh et al., 1994; Cook, 1996). Thus, knowledge of Sb aqueous speciation in ore-forming fluids and precipitation conditions of its solid phases is essential for both the use of Sb as an indicator in geochemical exploration, and the optimisation of hydrometallurgical processes of precious metals extraction from Sb-bearing ores and subsequent treatment and storage of Sb wastes (e.g., Ashley et al., 2003; Wilson et al., 2004). Another very promising feature of Sb geochemistry is large isotope variations discovered recently owing to the advances in multiple-collector inductively coupled plasma mass spectroscopy. For example, hydrothermal sulphide deposits exhibit a surprisingly wide range of $^{123}Sb/^{121}Sb$ compositions, up to 18 ε units ($\varepsilon^{123}Sb = 10{,}000 \times \{[^{123}Sb/^{121}Sb]_{sample}/[^{123}Sb/^{121}Sb]_{standard} - 1\}$), whereas in surface environments or magmatic rocks $^{123}Sb/^{121}Sb$ variations do not exceed 3–5 ε units (Rouxel et al., 2003). This can make Sb a potential geochemical tracer of both water–rock interactions and fluid sources. Knowledge of Sb oxidation state and identity and stability of its species in the fluid is a first requisite to interpreting Sb isotope signatures in hydrothermal systems.

Although pentavalent antimony, Sb^V, predominates in surficial environments, trivalent Sb^{III} is often present in significant amounts (see Filella et al., 2002; for a review). With increasing temperature and depth, Sb^{III} becomes by far the dominant oxidation state in volcanic and magmatic–hydrothermal fluids (Spycher and Reed, 1989; Zotov et al., 2003). On the basis of many solubility studies of Sb^{III} oxide and sulphide solids, aqueous hydroxide and sulphide complexes are believed to be the main Sb species in hydrothermal environments. Despite the somewhat uncertain stoichiometries for sulphide complexes which range from monomers to dimers according to different studies (e.g., Krupp, 1988; Spycher and Reed, 1989; Wood, 1989; Zotov et al., 1995), the majority of authors agree that sulfide species dominate only in H_2S-rich (>0.01–0.1 m) low-to-moderate temperatures (<200–250 °C) solutions of neutral-to-alkaline pH (Zotov et al., 2003; references therein). In most high-temperature hydrothermal fluids, the neutral Sb^{III} hydroxide, $Sb(OH)_3$, whose thermodynamic properties are well known to at least 450 °C, is believed to be largely responsible for Sb transport in a wide pH range (Zotov et al., 2003; references therein).

Most of these works, however, dealt with dilute solutions, often free of chloride, the major constituent of high-temperature fluids. In fact, it is well known from numerous ambient-temperature chemical studies (see Filella et al., 2002; for a review), and recent EXAFS measurements at elevated temperatures (Oelkers et al., 1998), that in concentrated HCl solutions (2–10 mol/kg), Sb^{III} does exhibit a strong chemical affinity for the Cl^- ligand by forming a range of chloride complexes, from $SbCl^{2+}$ to $SbCl_6^{3-}$, leading to enhanced solubilities of Sb solids. Despite the little relevance of these extremely acid solution compositions for natural environments, these data may also imply significance of Sb–Cl interactions in natural saline waters. Surprisingly, very few and rather contradictory studies exist about Sb speciation at elevated temperatures in Cl-rich geological fluids. Ovchinnikov et al. (1982) and Belevantsev et al. (1998) interpreted their stibnite solubility experiments in HCl–NaCl solutions from 170 to 300 °C by formation of Sb^{3+} together with a range of chloride species from $SbCl^+$ to $SbCl_4^-$. In contrast, Wood et al. (1987) observed no changes of stibnite solubility in slightly acidic to neutral NaCl solutions from 200 to 350 °C, which would be consistent with the predominance of $Sb(OH)_3$. The present study attempts to resolve these discrepancies and to better quantify the Sb–Cl interactions in natural chloride-bearing fluids on the basis of new X-ray absorption fine structure (XAFS) and solubility measurements.

In the last 15 years, the improvement of synchrotron sources and progress in high temperature–pressure ($T - P$) spectroscopic cell designs have provoked an "explosion" of X-ray absorption spectroscopy studies of local atomic structures of metals in high $T - P$ aqueous fluids (e.g., see Brown and Sturchio, 2002; for a recent review). These in situ data complemented by ab initio and molecular dynamics modelling (e.g., Sherman, 2001) provide unprecedented improvement of our knowledge of metal complexes stoichiometries and structures in hydrothermal fluids. However, because XAFS spectroscopy probes an average atomic environment around the absorbing atom, in many cases an ambiguity remains as for the true speciation, particularly in the case of a mixture of several complexes with different ligand numbers simultaneously present in the system. Moreover, owing to its very weak sensitivity to light atoms like proton, XAFS spectroscopy is not capable of detecting directly the charge of species formed through deprotonation/hydrolysis or complexation reactions. Thus, to derive unambiguously species identities and distribution from XAFS data in complex high-temperature aqueous systems, information about solubility of solid phases as a function of ligand concentration and/or pH is often required. High $T - P$ spectroscopic studies combining simultaneous measurement of mineral solubilities and local atomic structures are still very rare and dealt with simple systems (e.g., quartz–H_2O, Zotov and Keppler, 2002; GeO_2–H_2O, Pokrovski et al., 2005a).

In this work, we used a recently developed X-ray cell allowing simultaneous acquisition of XAFS transmission and fluorescence spectra in solution at high temperature and pressure to measure both Sb local atomic environment and senarmontite (Sb_2O_3, cub.) solubility in the system H_2O–NaCl–HCl to 450 °C and 600 bars. These new data were complemented by classical batch-reactor solubility measurements of Sb oxides and sulphide in a wide range of HCl and NaCl concentrations. The results obtained

evidence the formation of new mixed Sb hydroxy-chloride species dominant in ore-forming brines, and provide new insights into the nature and role of Sb–Cl interactions in high-temperature geological fluids.

2. Materials and methods

2.1. Experimental samples and conditions

Four XAFS experiments were performed on the following systems: Sb_2O_3(cub.)-pure water (Experiment 1, 250–400 °C, 600 bar), Sb_2O_3(cub.)–2.3 m[1] NaCl–0.1 m HCl aqueous solution (Experiment 2, 200-450 °C, 600 bar; and Experiment 3–4, 300–400 °C, 300 bar), and 0.1 m Sb(III)–3.5 m HCl aqueous solution (Experiment 5, 30–400 °C, 600 bar). Antimony trioxide was a natural cubic polymorph of Sb_2O_3 (senarmontite) from Algeria forming agglomerates of octahedral crystals (>2 mm) without detectable impurities (e.g., S, As < 1 wt%). Crystals were separated by hand, rinsed with de-ionized water, and passed in an ultrasonic bath with acetone to remove fine particles.

The XAFS experiments were complemented by three series of batch-reactor solubility measurements in the following systems: (A) Sb_2O_3 (rhomb., valentinite)–$NaClO_4$–$HClO_4 \pm NaCl$–H_2O (60 and 90 °C, P_{sat}), (B) Sb_2O_3 (cub., senarmontite)–NaCl–HCl–H_2O (300–400 °C, 300–600 bar), and (C) Sb_2S_3 (rhomb., stibnite)–NaCl–HCl–H_2O (300–400 °C, 150–600 bar). A few runs were also conducted at 300 °C in the system Sb_2O_3 (cub.)–$NaClO_4$–$HClO_4$–H_2O but they demonstrated Sb oxidation by perchlorate at this temperature yielding formation of servantite (Sb_2O_4, rhomb.) and Cl_2(g); they were not considered in the further analysis. Antimony trioxide used in the low-temperature runs (system A) was a powder of commercial rhombic polymorph, valentinite (Merck, >99%). For the high-temperature experiments (system B), this powder was aged for a week in contact with water at 350 °C and saturated vapor pressure (P_{sat}) in a titanium autoclave quenched in the end of the run. At temperatures above 300 °C in aqueous solution, valentinite is expected to transform rapidly into the thermodynamically stable cubic polymorph, senarmontite (Zotov et al., 2003). During quenching, re-precipitation of some valentinite could not be avoided however, so that the resulting solid contained about 10% of the rhombic phase as detected by X-ray diffraction. The solid was pressed in pellets for dissolution experiments at 300–400 °C. The presence of minor quantities of metastable valentinite in the solid was found to have no significant effect on the solubility above 300 °C which is controlled by the rapidly forming stable senarmontite. The last series of solubility experiments (system C) was conducted with natural stibnite (Sb_2S_3, rhomb.) from the Kadamjai Sb hydrothermal deposit (Tan-Shan Mountains, Turkmenia, Middle Asia). No trace metals like As, Cu, Ag, and Pb were detected by electron microprobe (<~0.5–1 wt%). Large stibnite crystals (1–5 cm) were cut in pieces of ~5 mm and cleaned ultrasonically in acetone. Aqueous solutions for all XAFS and solubility experiments were prepared from analytical-grade reagents and doubly de-ionized water.

2.2. XAFS spectra acquisition

XAFS spectra (including the X-ray absorption near edge structure region or XANES, and the extended X-ray absorption fine structure region or EXAFS) of antimony (III) aqueous solutions were collected in both transmission and fluorescence mode at Sb K-edge (~30.5 keV) over the energy range 30.3–31.5 keV on BM29 (Filipponi et al., 2000) and BM30B-FAME (Proux et al., 2005) bending-magnet beamlines at the European Synchrotron Radiation Facility (ESRF, Grenoble, France). The storage ring was operated at 6 GeV with a ~180 mA current. Energy was selected using either a Si(311) double-crystal monochromator detuned by 30% to eliminate higher order harmonics (on BM29) or a Si(220) double-crystal monochromator with sagittal focusing (on FAME). Contributions of higher order harmonics from the Si(220) double-crystal within the FAME optics configuration do not exceed 0.1% of the transmitted intensity in the energy and absorbance ranges of our experiments (Proux et al., 2006). The beam size was 300 μm horizontal × 500 μm vertical. X-ray photon flux on the sample was about 10^{10} photons/s at BM29 and 10^{12} photons/s at FAME. Ionization chambers filled with argon gas (BM29) or silicon diodes collecting scattered radiation from a Kapton foil (FAME) were employed for measuring the intensities of incident (I0) and transmitted (I1) X-ray beam. Fluorescence spectra were collected using a Canberra solid-state multi-element germanium detector.

XAFS experiments were carried out using a high temperature-pressure cell developed at the Laboratoire de Cristallographie (Grenoble) and recently described in detail elsewhere (Pokrovski et al., 2005a; Testemale et al., 2005). Briefly, the apparatus consists of an inner polycrystalline-sapphire or glassy-carbon optical cell heated externally by Mo electrical resistances and inserted in a high-pressure steel vessel. The vessel has a water-cooling jacket and three beryllium windows for X-ray passage. The autoclave is pressurized by helium gas with low absorption constant for X-rays. Preliminary experiments in the system Sb_2O_3 (cub.)–H_2O conducted on BM29 employed a polycrystalline sapphire inner cell with a sample space connected to a solution reservoir in the cold zone (see Pokrovski et al., 2005a; Testemale et al., 2005; for details). This led to Sb_2O_3 re-crystallization outside the heated space which prohibited both accurate solubility measurements and long-time EXAFS spectra acquisitions necessary to compensate for the low photon flux on BM29 beamline. Consequently, a new internal-cell design which avoids solid precipitation was developed, and the measurements described in this study were performed on FAME beamline.

[1] m denotes molality (i.e., the number of moles of solute per one kg of water in solution) through the entire article.

The new internal cell consists of a vertically oriented glassy-carbon tube (external diameter ~6 mm, internal diameter ~4 mm) polished inside, and two sapphire coaxial rods (diameter ~3.9 mm) inserted into the tube from its both ends and delimiting the sample space in which experimental solid and solution were placed (Fig. 1). The volume of the sample space is about 0.1–0.2 cm^3 which corresponds to a height of 3–6 mm. The sapphire rods have grooves in which Viton rubber joints are placed allowing the rods to move in the tube in response to pressure changes like a piston in a syringe. Pressure in the sample space is always balanced with that of He gas through the pistons. Thus, the optical path through the vertically oriented cell remains constant at high T and P owing to the low temperature expansion coefficient of glassy carbon, and fragile tube walls are never broken by stress. The temperature in the sample space is maintained within ±0.2 °C by Mo heating resistances and Pt–Pt/Rh thermocouples connected to a Eurotherm® temperature regulator. Temperature gradients through the sample space do not exceed 10 °C at an experimental temperature of 500 °C. Although the Viton seals are situated outside the heating zone (at ~100–150 °C when sample-space temperature is 500 °C) to avoid their thermal degradation, the relatively small 'dead-volume' space between rods and tube (<20–30% of the total volume) effectively hampers both solute diffusion and solid precipitation below or above the hot sample space. Senarmontite solubility is strongly temperature-dependent, decreasing by more than 3 orders of magnitude from 400 to 100 °C. As a result, after several hours above 300 °C in Experiments 2 and 3–4, some minor accumulation of Sb oxide at the internal side of the carbon tube in front of the large and colder fluorescence window was observed on the beam passage, resulting in poor spectra due to contributions both from the solution and solid. Nevertheless, this could easily be overcome by moving the autoclave by 0.1–0.2 mm closer to the fluorescence detector so that the beam passes again through the fluid phase only. The present cell design permits operating up to 500 °C and 1000 bar.

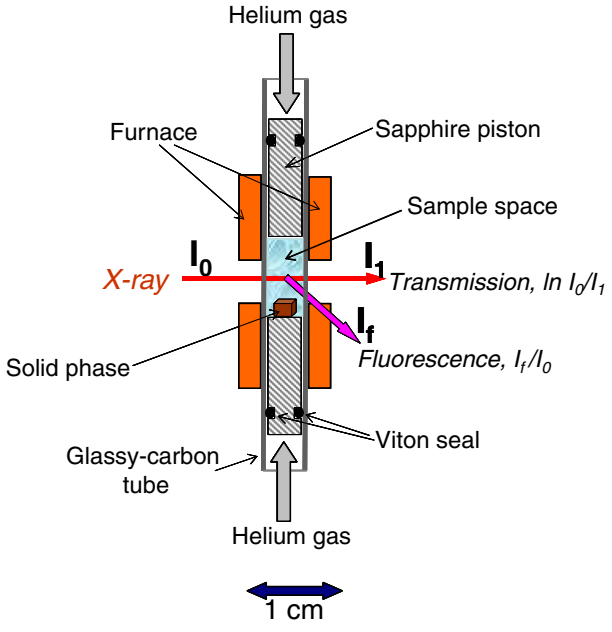

Fig. 1. Schematic drawing of the internal part of the X-ray cell used for XAFS measurements in this study.

Glassy-carbon tube material was found to be extremely inert at high temperatures in solutions ranging from pure water to concentrated NaCl–HCl. Dissolution tests in titanium-alloy batch reactors carried out on pieces of glassy carbon in the presence of Sb_2O_3 in pure water and HCl–NaCl aqueous solutions at 400 °C showed only weak dissolution of carbon (<0.01 mol. of dissolved C per kg of fluid after a two-week experiment) as determined by weight loss, and the absence of any redox reactions with antimony as evidenced by Scanning Electron Microscopy (SEM) of the solids after experiments.

In XAFS experiments in the presence of solid phase, a small senarmontite crystal (~20–50 mg, <1 mm in height) was placed at the bottom of the sample space below the beam passage through the solution (Fig. 1). The initial solid-to-solution mass ratio was about 1:4. Dissolution was studied at 300 and 600 bar from 150 to 450 °C by monitoring the Sb absorption-edge height in transmission mode as a function of time (see below). Simultaneously, fluorescence spectra were recorded. In the pure water system (Experiment 1) in which Sb concentrations ranged from 0.01 to 0.1 m, up to 5 scans (of ~50 min/scan data collection time) were collected and then averaged together at each temperature point after attainment of a steady-state. In the NaCl–HCl system (Experiments 2 and 3–4) where Sb concentrations were higher than 0.1 m, 2–4 scans were sufficient to obtain a low-noise EXAFS spectrum exploitable to 10–12 $Å^{-1}$ both in fluorescence and transmission modes.

2.3. XAFS data reduction

Data analysis was performed with the Athena and Artemis packages (Ravel and Newville, 2005) based on the IFEFFIT program (Newville, 2001). Details about the reduction procedure can be found elsewhere (Pokrovski et al., 2005a). Briefly, spectra were normalized to the absorption edge height, background-removed using the AUTOBK algorithm (Newville et al., 1993), weighted by k^n, where $n = 1$, 2 or 3, and Fourier filtered over the k range from ~3 to 10–12 $Å^{-1}$ (depending on signal-to-noise ratio) to produce radial structure functions (RSF). Fits were performed in the R-space on both real and imaginary parts of RSF contributions (Newville, 2001) to obtain the identity of the backscattering atoms, Sb-neighbor distance (R), coordination number (N), and the Debye–Waller factor (σ^2) for each scattering path (see Tables 1–3). In addition to these structural parameters, a non-structural parameter, Δe, was varied to account for the difference between the experimental absorption-edge energy and its estimate made by FEFF. To diminish correlations between N and σ^2, and better account for light versus heavy neighbors and multiple scattering paths, fits were performed simultaneously with k-weighting of 1, 2 and 3. The fitted

Table 1
Antimony(III) local structure in pure water in equilibrium with senarmontite (Sb_2O_3, cub.) as a function of temperature at 600 bar determined by fitting Sb K-edge EXAFS spectra (Experiment 1)

T (°C)	m_{Sb}	Scattering atom	N (atoms)	R (Å)	σ^2 (Å^2)	Δe (eV)	R-factor
250	0.010	O	3.0	1.961	0.0021	9.2	0.010
300	0.020	O	3.0	1.965	0.0030	9.3	0.006
350	0.043	O	2.9	1.965	0.0032	9.3	0.006
400	0.083	O	2.9	1.964	0.0035	9.2	0.008
Error of EXAFS fit			±0.3	±0.010	±30%	±1.5	

Concentrations are expressed in mol/kg of water (m_{Sb}); R, antimony-backscatterrer mean distance; N, number of neighbors; σ^2, squared Debye–Waller factor (relative to $\sigma^2 = 0$ adopted in the calculation of reference amplitude and phase functions by FEFF); Δe, non-structural parameter accounting for energy shift between experimental spectrum and FEFF calculation; R-factor, goodness of the total fit in R-space as described in FEFFIT (Newville, 2001). For all temperatures the fitted k- and R-ranges were, respectively, 2.6–11.0 Å^{-1} and 1.1–2.5 Å (not corrected for phase shift).

Table 2
Antimony(III) local structure in a 0.1 m Sb(III)–3.5 m HCl aqueous solution as a function of temperature at 600 bar determined by fitting Sb K-edge EXAFS spectra (Experiment 5)[a]

T (°C)	Scattering atom	N (atoms)	R (Å)	σ^2 (Å^2)	Δe (eV)	R-factor
30	Cl	2.1	2.43	0.005	8.5	0.010
150	Cl	2.1	2.42	0.006	8.4	0.029
200	Cl	2.6	2.42	0.007	8.9	0.015
250	Cl	2.4	2.41	0.007	8.8	0.022
300	Cl	2.5	2.41	0.007	9.2	0.011
400	Cl	3.0	2.39	0.007	9.2	0.003
Error of EXAFS fit		±0.3	±0.02	±30%	±1.0	

For all temperatures the fitted k- and R-ranges were, respectively, 3.6–10.0 Å^{-1} and 1.2–2.7 Å (not corrected for phase shift).
[a] See footnote of Table 1.

Table 3
Antimony(III) local structure in a 2.3 m NaCl–0.11 m HCl aqueous solution in equilibrium with senarmontite (Sb_2O_3, cub.) as a function of temperature and pressure determined by fitting Sb K-edge EXAFS spectra (Experiments 2 and 3–4)[a]

T (°C)	P (bar)	m_{Sb}	Scattering atom	N (atoms)	R (Å)	σ^2 (Å^2)	Δe (eV)	R-factor
200	610	0.0090	O	2.2	1.97	0.002	9.2	0.012
			Cl	0.5	2.47	0.007		
250	610	0.032	O	2.5	1.97	0.003	9.0	0.008
			Cl	0.4	2.43	0.008		
300	610	0.062	O	2.5	1.97	0.003	9.7	0.006
			Cl	0.4	2.41	0.008		
350	610	0.114	O	2.2	1.96	0.003	9.0	0.009
			Cl	0.4	2.41	0.010		
400	610	0.27	O	2.5	1.97	0.003	9.5	0.008
			Cl	0.3	2.39	0.010		
450	610	0.39	O	2.4	1.97	0.003	9.7	0.008
			Cl	0.4	2.37	0.016		
400	300	0.26	O	2.1	1.96	0.003	8.6	0.006
			Cl	0.4	2.40	0.009		
400	280	0.26	O	2.3	1.97	0.003	9.4	0.005
			Cl	0.4	2.41	0.009		
Error of EXAFS fit			O	±0.3	±0.01	±20%		
			Cl	±0.2	±0.02	±30%	±1.0	

For all temperatures the fitted k- and R-ranges were, respectively, 2.6–11.0 Å^{-1} and 1.1–2.6 Å (not corrected for phase shift).
[a] See footnote of Table 1.

values of structural parameters were identical within errors, with comparable fit qualities at each k-weighting. This is an additional demonstration of both the validity of the chosen structural models and the accuracy of the EXAFS background removal procedures (Ravel and Newville, 2005). Theoretical backscattering amplitude and phase-shift functions for Sb–O, Sb–H, Sb–Cl, and Sb–Sb single and multiple scattering paths were computed using the FEFF6 ab initio code (Zabinsky et al., 1995), using Sb_2O_3 and $SbCl_3$ crystal structures or $Sb(O,H,Cl)_m$–$(H_2O)_n$ model clusters. The amplitude reduction factor (S_0^2) was set at 0.95 ± 0.05 as found by fitting spectra of Sb_2O_3 and $SbCl_3$ solids. The influence of anharmonic disorder in determining structural parameters was checked using the cumulant expansion method (e.g., Crozier et al., 1988). The values of third- and fourth-order cumulants (c_3 and c_4) found when fitting the Sb first coordination shell, always converged to zero within error ($\pm 10^{-4}$). The presence of multiple scattering (MS) events within the Sb first coordination shell was also tested using the FEFF code, assuming local C_3 or T_d geometries around Sb, as found in the model compounds investigated. The MS contributions in the experimental EXAFS spectra of the studied systems were found to be negligible.

2.4. Determination of dissolved Sb concentration from the absorption edge height

Dissolved Sb concentrations were determined from the amplitude of the absorption-edge height over the Sb K-edge of transmission spectra ($\Delta\mu$) using the following equation based on the classical X-ray absorption relation (see Pokrovski et al., 2005a; for details):

$$C_{Sb} = \Delta\mu/(\Delta\sigma_{Sb}\ x\ M_{Sb}\ d_{fluid}), \quad (1)$$

where C_{Sb} is Sb aqueous concentration (mol kg^{-1} of solution), $\Delta\sigma_{Sb}$ is the change of the total absorption cross-section of Sb over its K-edge (cm^2 g^{-1}), x is the optical path length inside the cell (cm), M_{Sb} is Sb atomic weight (0.1218 kg mol^{-1}), and d_{fluid} is the density of the aqueous solution (g cm^{-3}) at given temperature and pressure.

The absorption cross-sections for Sb were taken from the recent compilation of Chantler et al. (2003). These values are in close agreement, within 2–5% below and above Sb K-edge, with other databases (e.g., as compiled in the Hephaestus software; Ravel and Newville, 2005).

The fluid density in the Sb_2O_3–H_2O experiment was calculated using the pressure–volume–temperature (PVT) properties of pure water (Kestin et al., 1984) and assuming that the low concentrations of dissolved Sb, C and Al ($m_{Sb} < 0.1$; $m_C < 0.01$; $m_{Al} < 0.0001$) do not significantly modify these properties. This assumption is supported by recent high-temperature in situ volumetric measurements on aqueous solutions of antimonious acid analogs, arsenious and arsenic acids, which show that density differences between a 0.1 m As solution and pure water do not exceed 2% of the value in the range 20–350 °C (Perfetti, 2003). For the Sb–NaCl–HCl experiments, where Sb dissolved concentrations attain ~0.4 m, the fluid density was calculated using the PVTX properties of the NaCl–H_2O system (Anderko and Pitzer, 1993; Bakker, 2003) and assuming that a given weight concentration (wt%) of dissolved Sb yields the same contribution to the fluid density as the equivalent weight concentration of NaCl. The density contribution of dissolved Sb calculated using the above assumption does not exceed 0.07 g/cm^3 at 0.4 m Sb for total fluid densities greater than 0.65 g/cm^3. Densities of the 0.1 m Sb–3.5 m HCl solution (Experiment 5) up to 200 °C were taken as those reported for the HCl–H_2O system (Zaytsev and Aseyev, 1985), and extrapolated to higher temperatures using an analogy with NaCl–H_2O solutions of the same weight concentration. The maximal error of density estimations using the approximations above does not exceed 10% of the value at temperatures above 250 °C.

The height of the absorption-edge step ($\Delta\mu$) in each XAFS scan was determined using a classical 'empirical' normalization technique of the AUTOBK algorithm (Newville et al., 1993), and an independent Cromer–Liberman normalization (CLnorm, Cromer and Liberman, 1970), both implemented in the Athena software (Ravel and Newville, 2005). Values of $\Delta\mu$ found using both approaches were identical within errors, thus confirming the validity of estimates of atomic-like background over Sb K-edge. The uncertainty on $\Delta\mu$ determination, as evaluated by changing fitted energy ranges or by comparing different scans with the same Sb concentration, varies from less than 1% to 2% of the total value for absorption steps greater than 0.1 (which roughly corresponds to 0.05–0.1 m of dissolved Sb), to about 10% for absorption steps between 0.01 and 0.02 (~0.01 m Sb).

The validity of Eq. (1) is demonstrated by Experiment 5 carried out on a 0.1 m Sb–3.5 m HCl solution which is stable over a wide temperature range (e.g., Oelkers et al., 1998). Antimony concentrations derived at temperatures from 150 to 400 °C using Eq. (1) are identical to the nominal value at 30 °C within errors (Table 4). Fig. 2 shows transmission XAFS scans recorded during this experiment as a function of temperature at 600 bar. The decrease of the before-edge absorption follows the drop of the fluid density with temperature (the relative contribution of Sb absorption to the before-edge is almost constant, ~15% of the total absorption), whereas the absorption-edge height corresponds to Sb solution concentration according to Eq. (1). The total absorption values and spectra shape and amplitude at a given temperature are well reproducible both on heating and cooling.

Table 4
Antimony aqueous concentrations in equilibrium with senarmontite in pure water (Experiment 1) and 2.3 m NaCl–0.11 m HCl solution (Experiments 2 and 3–4), and in 3.5 m HCl solution without solid phase (Experiment 5), derived from the edge height of X-ray absorption spectra at Sb K-edge as a function of temperature and pressure[a]

T (°C)	P (bar)	d_{fluid} (g/cm^3)	$\Delta\mu$[b]	C_{Sb}[c] (mol/kg of fluid)	$\log_{10} m_{Sb}$[d]
Experiment 1: Sb_2O_3(cub)–H_2O					
250	610	0.851	0.012	0.0094	−2.03 ± 0.10
300	610	0.789	0.024	0.020	−1.70 ± 0.10
350	610	0.713	0.049	0.045	−1.35 ± 0.05
400	610	0.615	0.077	0.082	−1.08 ± 0.05
Experiment 2: Sb_2O_3(cub)–2.3 m NaCl–0.11 m HCl					
200	610	0.993	0.012	0.0080	−2.04 ± 0.10
250	610	0.950	0.041	0.028	−1.49 ± 0.10
300	610	0.900	0.075	0.054	−1.21 ± 0.05
350	610	0.856	0.153	0.12	−0.87 ± 0.05
400	610	0.802	0.278	0.23	−0.57 ± 0.07
450	610	0.735	0.363	0.32	−0.41 ± 0.10
Experiment 3–4: Sb_2O_3(cub)–2.3 m NaCl–0.11 m HCl					
300	307	0.890	0.107	0.079	−1.04 ± 0.10
400	304	0.760	0.253	0.22	−0.59 ± 0.10
Experiment 5: 0.1m Sb-3.5m HCl					
30	605	1.082	0.162	0.098[a]	−0.950 ± 0.005
150	632	0.978	0.153	0.103	−0.93 ± 0.05
200	612	0.966	0.148	0.101	−0.94 ± 0.08
250	611	0.900	0.143	0.104	−0.92 ± 0.10
300	610	0.844	0.136	0.106	−0.92 ± 0.10
400	610	0.691	0.099	0.094	−0.97 ± 0.10
300	610	0.840	0.135	0.105	−0.92 ± 0.10
200	600	0.966	0.148	0.100	−0.94 ± 0.10
150	600	0.978	0.154	0.103	−0.93 ± 0.10

[a] The X-ray beam path inside the cell was set at 0.38 ± 0.02 cm based on Eq. (1), Sb initial concentration of 0.098 ± 0.001 mol/kg solution, density of 3.5 m HCl at 30 °C/600 bar, and change of antimony total absorption cross-section, σ, over Sb K-edge of 33.84 cm^2 g^{-1} (Chantler et al., 2003).
[b] Height of the absorption jump over Sb K-edge as derived from transmission XAFS spectra.
[c] Sb total dissolved concentration (in mol/kg of solution) calculated using Eq. (1).
[d] Logarithm of Sb molality (mol/kg H_2O). Uncertainties on the values stem from those associated with the determination of the absorption edge height, X-ray path length, and solution density (see text).

2.5. Batch-reactor solubility measurements

The results of valentinite solubility measurements at 60 and 90 °C (series A) and their detailed analysis are reported in Electronic Annex (EA). Senarmontite and stibnite solubility experiments from 300 to 400 °C (series B and C) were conducted using ~20 cm^3 titanium alloy (Ti, Mo and Al) reactors placed in a temperature controlled (±1 °C) furnace. Details about this technique are described elsewhere

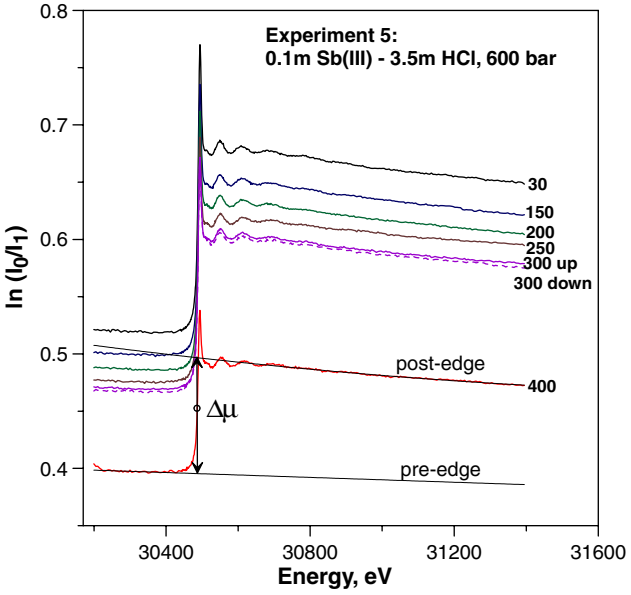

Fig. 2. Raw XAFS transmission scans at Sb K-edge of a 0.1 m Sb-3.5 m HCl aqueous solution (Experiment 5) at 600 bar and indicated temperatures (in °C). An example of edge height determination ($\Delta\mu$) using the AUTOBK algorithm is shown on the 400 °C spectrum (see text). The decrease of the before-edge absorption with increasing temperature follows the corresponding decrease of water density (largest changes occurring between 300 and 400 °C), whereas the absorption edge height is a measure of Sb concentration in the fluid according to Eq. (1).

(Pokrovski et al., 2002a). Briefly, the solid phase was put in a titanium holder fixed in the upper part of the reactor so that it does not contact the solution at ambient temperature. Initial solid-to-solution ratios were in the range 1:100–1:20. Experimental pressures were calculated from the degree of filling of the autoclave and using the PVTX properties of the $H_2O \pm NaCl$ system as described above (Section 2.4). At the end of each run, the reactor was quenched in cold water to rapidly separate solid from solution. The dissolved Sb contents were determined from the weight loss of the solid phase. It was found that steady-state concentrations were attained after 4 days in Sb_2O_3 runs and a week in Sb_2S_3 experiments. X-ray diffraction and SEM analyses of solid phases after Sb_2O_3–HCl–NaCl runs at high HCl concentration (0.1 m) at 300 °C showed the presence of senarmontite, onoratoite ($Sb_8O_{11}Cl_2$), and other unidentified Sb oxy-chloride phases. Despite the dominant presence of senarmontite which likely remains the solubility-controlling phase, an ambiguity in the weight-loss interpretation and final Cl concentration in solution in the presence of such oxy-chloride phases did not allow to use these experiments in further thermodynamic analyses. In contrast, low-acidity experiments (H_2O–NaCl) at 300 °C and all experiments at 350 and 400 °C in the system Sb_2O_3–HCl–NaCl showed the only presence of senarmontite. In the Sb_2S_3–HCl–NaCl runs, stibnite also remained unchanged and no new phases were detected over the entire temperature–composition range investigated.

3. Results from XAFS spectroscopy

3.1. Local structure of antimony(III) in aqueous solution

XANES spectra of *pure-water solutions saturated with Sb_2O_3 from 250 to 400 °C at 600 bar (Experiment 1)* exhibit identical edge-crest energies and spectral shapes (not shown). The magnitudes of the white line of normalized spectra for all solutions recorded both in transmission and fluorescence modes were the same, thus demonstrating the absence of self-absorption in fluorescence spectra. The spectral shape and energy position of the aqueous samples are similar to those of the cubic Sb_2O_3 solid, thus suggesting a similar pyramidal SbO_3 geometry around Sb(III) in solution. This is confirmed by the analysis of EXAFS spectra which show a single-shell contribution (Fig. 3) from 3 ± 0.3 oxygen atoms at 1.965 ± 0.010 Å around Sb over the temperature range investigated (Table 1). These structural parameters are in excellent agreement with previous solubility studies (Zotov et al., 2003; references therein) which suggest the formation of the neutral $Sb(OH)_3^\circ$ complex in a wide pH–temperature range (note that EXAFS is not capable of seeing hydrogen atoms in most cases). The constancy of Sb–O distances and coordination numbers and low disorder (DW factors) in a wide temperature–density range are similar to that for analogous aqueous hydroxide complexes like $As(OH)_3^\circ$ and $Ge(OH)_4^\circ$ which show no detectable changes in metal-oxygen bond distances in aqueous solution from ambient temperature to at least 400–500 °C (Pokrovski et al., 2002b, 2005a; Testemale et al., 2004). Thus, due to a strong covalent character of the Sb–O bonds (Pauling, 1948) and the absence of significant hydration by outer-sphere water molecules typical of metal cations and charged complexes, the increasing thermal vibration with temperature has negligible effect on the inter-atomic distances and the structure of the neutral $Sb(OH)_3$ species.

XANES spectra of *0.1 m Sb(III) in 3.5 m HCl solution (Experiment 5)* show no detectable changes from 30 to 400 °C at 600 bar and are similar both in shape and energy position to crystalline $SbCl_3$. Representative examples of EXAFS spectra are shown in Fig. 3. Their modeling yields a single-shell contribution from ~2 to ~3 (±0.3) Cl atoms around Sb with average Sb–Cl distances decreasing from 2.43 to 2.39 (±0.02) Å when temperature rises from 30 to 400 °C (Table 2). These values and their temperature evolution are in excellent agreement with those reported in a similar EXAFS study of 2–3 m HCl antimony chloride solutions from 25 to 250 °C at P_{sat} (Oelkers et al., 1998). They are consistent with the formation of $SbCl_n^{3-n}$ complexes widely documented in chemical literature at ambient temperature in highly concentrated HCl solutions (e.g., Oelkers et al., 1998; Filella et al., 2002; references therein). An increase with temperature of the average number of Cl neighbors around Sb (from 2.1 at 30–150 °C to 2.5 at 200–300 °C), particularly pronounced at 400 °C (3.0), as

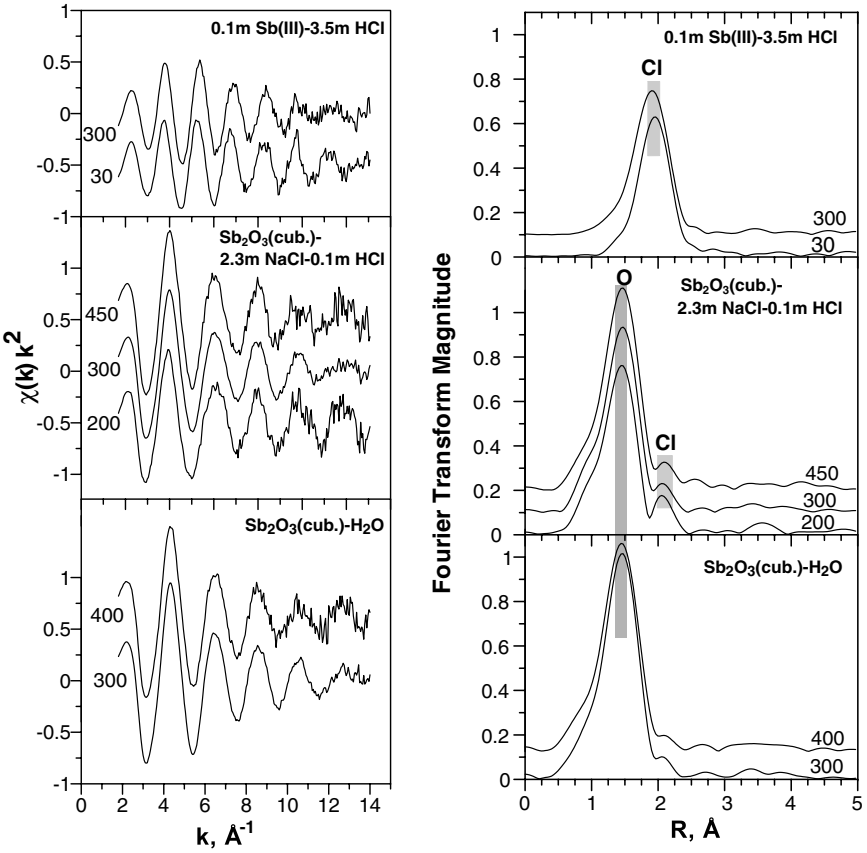

Fig. 3. Normalized k^2-weighted fluorescence EXAFS spectra of Sb(III)-bearing aqueous solutions with compositions indicated in the Figure, at 600 bar and selected temperatures (in °C), and their corresponding Fourier transform magnitudes (not corrected for phase shift). Grayed bands indicate positions of oxygen (O) and chlorine (Cl) nearest neighbors around the Sb atom as found by fitting EXAFS spectra (see Tables 1–3). Spectra are shifted along the vertical axis for clarity.

observed in our study, suggests an increase in stability of larger and less charged species, likely $SbCl_3^\circ$ at the expense of $SbCl_2^+$. This is consistent with the decrease of the fluid dielectric constant at high temperature that favors ion association and thus neutral species stability. The decrease of Sb–Cl bond length with increasing temperature is similar to that observed for other metal-chloride aqueous species like $Cu^{II}Cl_{2-3}$ (Collings et al., 2000), $ZnBr_{2-4}$ (Mayanovic et al., 2001; Simonet et al., 2002), and $InCl_{3-4}$ (Seward et al., 2000). These changes are in agreement with the temperature evolution of solvent hydrogen bonding, and solvent–solute interactions including such factors as dielectric saturation and solvent compressibility (e.g., Shock et al., 1992; Oelkers et al., 1998). Because of the weakening with increasing temperature of the hydration by outer-sphere water molecules which tend to pull ligands out from the metal, Sb–Cl bonds are expected to become 'tighter' and thus shorter at higher temperature. Note that the 2.39 ± 0.02 Å Sb–Cl distance detected in our solution at the highest temperature studied (400 °C) is close to that in gas-phase $SbCl_3$ ($R_{Sb-Cl} = 2.37 \pm 0.02$ Å, Allen and Sutton, 1950) and in crystalline antimony tri-chloride whose structure consists of discrete $SbCl_3$ molecules ($R_{Sb-Cl} = 2.35 \pm 0.01$ Å, Lipka, 1979). This provides a further support for the stoichiometry of the dominant $SbCl_3^\circ$(aq) complex which interacts only weakly with the solvent at high temperatures.

Selected EXAFS spectra of *0.1 m HCl–2.3 m NaCl solution saturated with senarmontite (Experiment 2)* and their RSF are presented in Fig. 3. Spectra recorded in fluorescence and transmission (where $m_{Sb} > 0.1$) modes were very similar and yielded identical structural parameters. It can be seen in Fig. 3 that two contributions are apparent in the Fourier transform which implies the presence of both oxygen and chlorine atoms in the Sb nearest coordination shell. No more distant shells were detected. The average numbers of O and Cl are 2.3 ± 0.2 and 0.4 ± 0.2 atoms, respectively, over the entire range of temperature (200–450 °C) and Sb concentrations (~0.01–0.40 m, see Table 3). Average Sb–O distances remain constant at these conditions (1.97 ± 0.01 Å) and are identical within errors to those of the $Sb(OH)_3^\circ$(aq). In contrast, mean Sb–Cl bond lengths decrease from 2.47 to 2.37 (±0.02) Å when temperature increases from 200 to 450 °C. These values and their temperature changes are very similar to those found for the $SbCl_{2-3}$ species in the 3.5 m HCl solution (Experiment 5, see above). Because of the average nature of an EXAFS signal, Sb speciation in our NaCl–HCl solution can be interpreted either by a mixture of purely hydroxide and chloride species similar to those found in

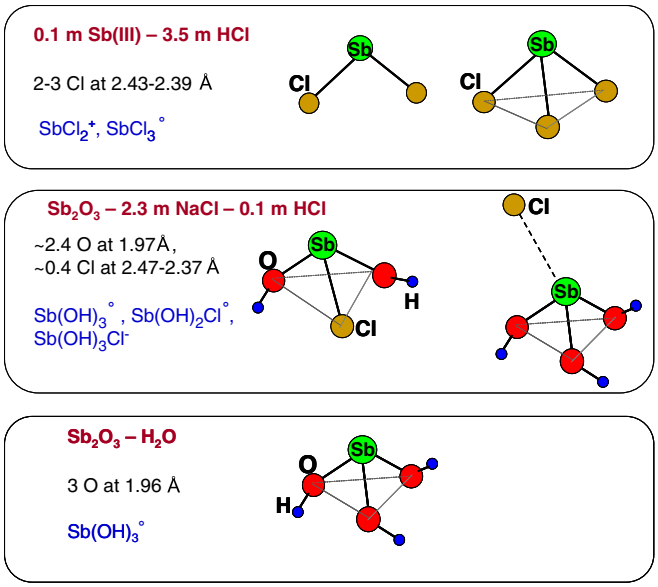

Fig. 4. Stoichiometries and schematic structures of the dominant Sb(III) aqueous species found in the XAFS experiments of this study.

pure water and concentrated HCl, respectively, or by new mixed hydroxy-chloride complexes (Fig. 4). Since EXAFS alone does not allow us to choose between these two possibilities, it was complemented by linear combination fit (LCF) analysis as implemented in the Athena program. Modeling of the XANES spectra of the Sb–NaCl–HCl solution using different proportions of $Sb(OH)_3$ (from Experiment 1) and $SbCl_3$ (from Experiment 5) chosen as reference end-members resulted in poor regression statistics and unstable fits, with $SbCl_3$ contributions ranging from 0.05 to 0.4 which would correspond to Cl coordination numbers from 0.1 to 1.2. Because the XANES part of the spectrum is much more sensitive to the cluster geometry than EXAFS, poor fitting using pure Sb–O and Sb–Cl end-members is likely not consistent with a mixture of purely hydroxide and chloride species, but rather indicates the presence of mixed Sb–(OH)–Cl complexes with distinct XANES spectra. In contrast, LCF regressions in the chi-space of EXAFS spectra using the same references yielded $Sb(OH)_3$ and $SbCl_3$ contributions of 0.7–0.8 and 0.07–0.20 corresponding to O and Cl average coordination numbers of 2.3 ± 0.2 and 0.4 ± 0.2, respectively. This is in perfect agreement with the values derived from the classical EXAFS analysis (see above and Table 3). However, more direct and quantitative interpretation of Sb speciation in this solution is achieved by combining EXAFS structural parameters with measured solubilities.

3.2. XAFS-derived solubility of senarmontite in pure water and a 2.3 m NaCl–0.1 m HCl solution

The evolution of Sb absorption edge height of transmission spectra ($\Delta\mu$) with temperature and time for consecutive scans during senarmontite dissolution experiments 1 (pure water) and 2 (NaCl–HCl) is shown in Fig. 5. It can be seen that steady-state values for the absorption-edge height in pure water are attained within an hour below 300 °C, and ~2 h at higher temperature (Fig. 5a). In the NaCl–HCl solution, the dissolution was somewhat faster, with a steady-state achieved within an hour after each temperature rise from 150 to 450 °C. Note that these values are reproducible on cooling for both experiments (Fig. 5). Antimony steady-state concentrations derived from the edge height values using Eq. (1) are reported in Table 4 and compared with other available data in Fig. 6. In pure water, our concentrations are in very good agreement both with our own batch-reactor solubility measurements (Table 5) and the HKF-model predictions of Zotov et al. (2003) using the thermodynamic properties of $Sb(OH)_3^\circ(aq)$ derived from a large set of solubility data for Sb, Sb_2O_3 and Sb_2S_3. In the NaCl–HCl solution, the XAFS-derived Sb concentrations are in excellent agreement with batch-reactor solubilities of senarmontite measured in this study (Fig. 6, Table 5). These results strongly suggest that the solid-solution equilibrium was attained in our XAFS experiments.

Thus, both XAFS and solubility data on pure-water solutions in equilibrium with senarmontite clearly demonstrate the dominant presence of the neutral $Sb(OH)_3$ species formed according to the reaction:

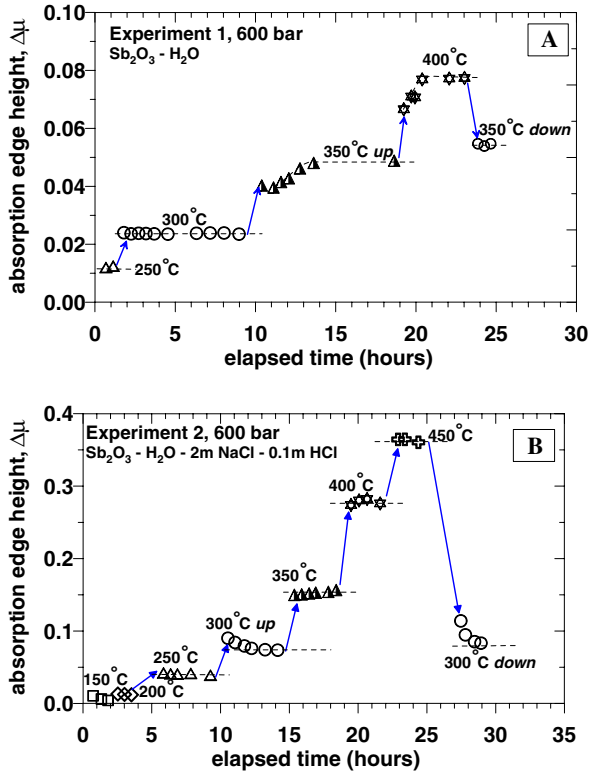

Fig. 5. Evolution of the absorption edge height of transmission spectra of aqueous Sb as a function of time and temperature in (A) Experiment 1 (senarmontite-pure water) and (B) Experiment 2 (senarmontite—2.3 m NaCl–0.1 m HCl solution). Each symbol corresponds to a XAFS scan. Arrows indicate temperature changes during the experiment; dashed lines linking the symbols at a given temperature are drawn to guide the eye. Error bars are about the symbol size.

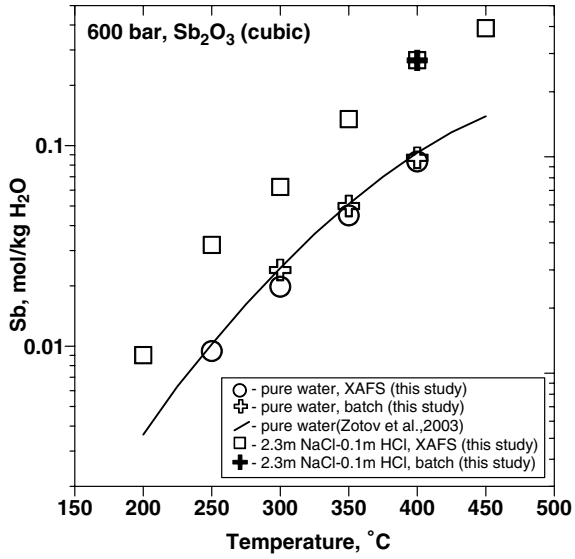

Fig. 6. Solubility of cubic antimony trioxide (senarmontite) in pure water and a 2.3 m NaCl–0.1 m HCl solution versus temperature at 600 bar. Symbols correspond to measurements performed in this work using both in situ XAFS spectroscopy and weight-loss batch-reactor technique. Uncertainties do not exceed the symbol size. The curve was generated using the thermodynamic properties of senarmontite and $Sb(OH)_3^\circ(aq)$ reported by Zotov et al. (2003).

$$0.5\ Sb_2O_3\ (cub.) + 1.5\ H_2O = Sb(OH)_3^\circ(aq). \quad (2)$$

Assuming activity coefficients of neutral species close to one, the equilibrium aqueous concentration of $Sb(OH)_3$ is equal to the reaction constant ($K_2 = m_{Sb(OH)_3}$), and is independent of solution composition at given temperature and pressure. Thus, in the investigated NaCl–HCl solution in equilibrium with senarmontite, $Sb(OH)_3$ concentration remains constant and equal to that in pure water at each T and P. Consequently, the ~3-fold senarmontite solubility increase measured from 200 to 450 °C in this solution in comparison to pure water can be attributed to the formation of other hydroxide and/or chloride species. Combining the measured solubilities in the NaCl–HCl solution and pure water with average numbers of O and Cl atoms around Sb in both solutions derived from the EXAFS analysis at each temperature, we conclude that mixed monochloride complexes $Sb(OH)_nCl$ with n from 2 to 3 are likely to account for the observed solubility increase over the entire temperature range investigated. The amounts of $Sb(OH)_3$ (which represents ~30% of the total Sb concentration in the 2.3 m NaCl–0.1 m HCl solution, see Table 4) and $Sb(OH)_2Cl$ accounting for the remaining dissolved Sb, correspond to an average oxygen number of 2.3 around Sb,[2] in perfect agreement with the EXAFS results (see Table 3). The average numbers of Cl in such a mixture of $Sb(OH)_3$ and $Sb(OH)_2Cl$, $N_{Cl} \sim 0.6$–0.7, are somewhat higher than those found from EXAFS spectra for this solution ($N_{Cl} \sim 0.3$–0.5). Despite large uncertainties usually associated with EXAFS-derived coordination numbers, this might imply a contribution to the solubility from other Cl-bearing species like $Sb(OH)_3Cl^-$ in which the negatively charged Cl^- anion is bound to the pyramidal $Sb(OH)_3$ via the Sb summit having a positive partial charge (Fig. 4). It is likely that a large disorder associated with such electrostatic Sb–Cl bond may not allow its detection by EXAFS. An analogous outer-sphere silicic acid–sulfate species, $Si(OH)_4(SO_4)^{2-}$, was proposed to account for the elevated silica solubilities in sodium sulfate solutions at high temperatures (Marshall and Chen, 1982). Another possible species consistent with the EXAFS-derived numbers of oxygen would be $Sb(OH)_2^+$ which is known to form at strongly acid pH (Baes and Mesmer, 1976). However, its stability constants derived from low-temperature measurements imply its negligible contribution (<5% of total Sb) in our NaCl–HCl solution above 200 °C (Electronic Annex). Note also that the dominant formation in Experiments 2 and 3–4 of chloride species like $SbCl_{1-4}$ and/or Sb^{3+}, as suggested by Ovchinnikov et al. (1982) to explain Sb_2S_3 solubilities in similar NaCl–HCl solutions, can be excluded because it would have implied too low O (<1.5 atom) and too high Cl (>1 atom) average coordination numbers not compatible with our XAFS data. Thus, it is very likely that mixed hydroxy-chloride species are responsible for the elevated Sb_2O_3 and Sb_2S_3 solubilities in acidic NaCl solutions in a wide temperature range.

4. Stoichiometry and stability of Sb(III) hydroxy-chloride complexes in high-temperature saline fluids

4.1. Conventions, units and standard states

In this study, Gibbs free energies of minerals and aqueous species are represented as apparent standard molal Gibbs free energies ($\Delta G^\circ_{P,T}$) of formation from the elements at the subscripted pressure (P) and temperature (T) (Tanger and Helgeson, 1988). The reference states for the elements (for which $\Delta G^\circ_{1\ bar,298\ K} = 0$) in the system Sb–O–H–S–Cl are elemental antimony and sulphur, O_2, ideal gas, H_2, ideal gas, and Cl_2, ideal gas. The standard states for the solid phases and H_2O are unit activity for the pure phase at all temperatures and pressures. For aqueous species, the reference state convention corresponds to unit activity coefficient for a hypothetical 1 molal solution whose behavior is ideal. Aqueous species concentrations are expressed in molal units (mol/kg H_2O) and equilibrium constants are given in the molality scale. Activity coefficients (γ_i) of charged species were calculated using the extended Debye–Hückel equation:

$$\log \gamma_i = -A\ z_i^2 \sqrt{I}/(1 + B\ \mathring{a}_i\ \sqrt{I}) + \Gamma_\gamma + b_{NaCl}\ I, \quad (3)$$

where A and B refer to the Debye–Hückel electrostatic parameters and were taken from Helgeson and Kirkham

[2] For a mixture of $Sb(OH)_3$ and $Sb(OH)_2Cl$ in solution of Experiment 2, the average numbers of O (N_O) and Cl (N_{Cl}) around Sb are calculated as follows: $N_O = (3 * m_{Sb1} + 2 * (m_{Sb2} - m_{Sb1}))/m_{Sb2}$, and $N_{Cl} = (m_{Sb2} - m_{Sb1})/m_{Sb2}$, where m_{Sb1} and m_{Sb2} = total Sb molalities measured in Experiment 1 and 2, respectively.

Table 5
Solubility of senarmontite (Sb_2O_3, cub.) in NaCl–HCl aqueous solutions at 300, 350 and 400 °C as determined by the weight-loss method from batch-reactor experiments

Run	T (°C)	P (bar)	Duration (days)	Mass of fluid (g)	Weight loss of Sb_2O_3 (g)	HCl (mol/kg H_2O)	NaCl (mol/kg H_2O)	Sb (mol/kg H_2O)
9	300	330	12	14.646	0.051	0	0	0.024
R5	300	300	19	16.260	0.063	0	0	0.027
R103	300	300	19	15.140	0.064	0	1.07	0.029
11	300	300	12	16.662	0.095	0	2.28	0.044
1	350	300	4	21.313	0.152	0	0	0.049
8	350	300	10	21.344	0.162	0	0	0.052
5	350	300	7	30.681	0.410	0	5.30	0.120
6	350	300	7	30.286	0.356	0	3.91[a]	0.104
7	350	300	10	21.384	0.182	0.0017	0	0.059
3	350	300	4	23.923	0.256	0.0145	1.19	0.078
4	350	300	7	30.646	0.532	0.0175	5.28	0.156
2	350	300	4	26.329	0.630	0.0927	2.65	0.189
400-4	400	580	4	9.415	0.120	0	0	0.087
400-3	400	580	4	16.715	0.597	0.118	2.34	0.255
400-2	400	600	4	11.244	0.369	0.118	2.34	0.278

[a] KCl was used instead of NaCl.

(1974); I is the effective molal ionic strength ($I = 0.5 \sum z_i^2 m_i$); z_i and $\mathring{a}_i$ represent the ionic charge and the distance of the closest approach for ith species, respectively; Γ_γ designates the mole fraction to molality conversion factor, $\Gamma_\gamma = \log(1 + 0.018\, m^*)$, where m^* stands for the sum of the molalities of all solute species; and b_{NaCl} is the extended term parameter for NaCl-dominated solutions, which is a function of temperature and pressure (Oelkers and Helgeson, 1990). We adopted a value for $\mathring{a}_i$ of 4.5 Å for all charged species. For activity coefficients of neutral species, Eq. (3) reduces to $\log \gamma_i = \Gamma_\gamma + b_i I$, where b_i is the empirical Setchenov coefficient for each neutral complex. Because of the extreme scarcity of Setchenov coefficients for different neutral species, a zero value for b_i was adopted in the present study which yields activity coefficients for all neutral species close to one.

4.2. Interpretation of the solubilities of senarmontite and stibnite in NaCl–HCl solutions

Because the limited number of our XAFS experiments does not allow unambiguous derivation of stoichiometries and stabilities for the dominant Sb aqueous complexes over the range of Cl contents of natural fluids, the XAFS data were complemented by batch-reactor solubility measurements of stibnite and senarmontite in aqueous solution from 300 to 400 °C and from 150 to 600 bar in a wide range of NaCl (0–5 m) and HCl (0–0.2 m) concentration. The results are reported in Tables 5 and 6. In their interpretation, we considered a number of possible hydroxy-chloride and chloride complexes in acid to neutral aqueous solutions ($\sim 1.5 < pH < \sim 7$) formed according to the reactions:

$$Sb(OH)_3^\circ(aq) + Cl^- = Sb(OH)_3Cl^- \quad (4)$$

$$Sb(OH)_3^\circ(aq) + Cl^- = Sb(OH)_2Cl^\circ(aq) + OH^- \quad (5)$$

$$Sb(OH)_3^\circ(aq) + 2Cl^- = Sb(OH)Cl_2^\circ(aq) + 2OH^- \quad (6)$$

$$Sb(OH)_3^\circ(aq) + 3Cl^- = SbCl_3^\circ(aq) + 3OH^- \quad (7)$$

$$Sb(OH)_3^\circ(aq) + Cl^- = Sb(OH)Cl^+ + 2OH^- \quad (8)$$

$$Sb(OH)_3^\circ(aq) + 2Cl^- = SbCl_2^+ + 3OH^- \quad (9)$$

Our choice of the Sb–OH–Cl species stoichiometries was guided by the XAFS data on 3.5 m HCl and 2.3 m NaCl–0.1 m HCl solutions (see above), and previous solubility studies in Cl-free fluids showing the dominant presence of $Sb(OH)_3^\circ(aq)$ (Zotov et al., 2003; references therein). Although species with higher charges and/or bigger ligand numbers like $SbCl^{2+}$, $SbCl_4^-$, $SbCl_5^{2-}$ or $SbCl_6^{3-}$ detected in 3–10 m HCl solutions at ambient temperatures (e.g., Milne, 1975) cannot be completely excluded, their significant amounts at the elevated temperatures and moderate acidities of our experiments seem very unlikely, following the dramatic decrease of the fluid dielectric constant with increasing temperature which favors ion association and stability of neutral or weakly charged species (e.g., Crerar et al., 1985). Moreover, their dominant presence even in 3.5 m HCl solution (Experiment 5) would have been inconsistent with the average Cl numbers derived from XAFS. Thus, we did not consider such species in the solubility analysis.

In addition, the $Sb(OH)_2^+$ cation, which was shown to form at very acid pH (<2) at low temperatures, was also included in the speciation scheme, but was found to represent less than 5% of total Sb in the most acid solutions (0.2 m HCl) used in our solubility measurements (see Electronic Annex). The formation of less hydrolyzed Sb(III) cations like Sb^{3+} and $Sb(OH)^{2+}$ can be neglected at high temperatures both on the basis of our EXAFS results and their stability constants reported at ambient conditions (Baes and Mesmer, 1976; Filella and May, 2003) which imply negligible amounts of these species in comparison to

Table 6
Solubility of stibnite (Sb_2S_3, rhomb.) in NaCl–HCl aqueous solutions at 300 and 400 °C as determined by the weight-loss method from batch-reactor experiments

Run	T (°C)	P (bar)	Duration (days)	Mass of fluid (g)	Weight loss of Sb_2S_3 (g)	HCl (mol/kg H_2O)	NaCl (mol/kg H_2O)	Sb (mol/kg H_2O)
S3/23	300	560	8	11.777	0.0053	0	0	0.0026
S7/23	300	580	17	11.803	0.0056	0	0	0.0028
S13/1	300	580	17	19.790	0.0110	0	2.279	0.0037
S12/104	300	580	17	16.835	0.0184	0.0343	2.282	0.0073
S8/24	300	580	17	12.391	0.0088	0.0361	0.360	0.0043
S15/5	300	130	17	16.160	0.0240	0.0361	0.360	0.0089
S9/25	300	580	17	13.389	0.0294	0.104	0.360	0.013
S14/4	300	550	17	18.598	0.0551	0.108	1.080	0.019
S10/101	300	590	17	16.948	0.0604	0.115	2.278	0.024
S5/101	300	600	14	16.981	0.0670	0.114	2.321	0.026
S11/103	300	570	17	16.738	0.1102	0.232	2.308	0.044
SS1/25	403	590	13	10.025	0.0302	0	0	0.018
S16/24	399	450	6	11.210	0.0318	0	2.272	0.019
SS8/23	403	570	13	12.229	0.0440	0	2.287	0.024
SS3/103	403	600	13	15.150	0.0550	0.0110	2.255	0.024
SS4/104	403	580	13	16.273	0.0903	0.0345	2.283	0.037
SS5/5	403	590	13	15.477	0.141	0.109	1.088	0.057
SS6/1	403	400	13	16.331	0.156	0.116	2.296	0.064
S17/25	399	600	5	12.675	0.130	0.115	2.301	0.069
SS7/24	403	580	13	12.351	0.111	0.116	2.295	0.060
SS2/101	403	560	13	14.333	0.226	0.235	2.337	0.106

$Sb(OH)_2^+$ and $Sb(OH)_3^\circ$ at acidities lower than 1 mol H^+. The presence of Sb sulfide complexes in the Sb_2S_3 solubility runs was also tested using their available stability constants (Krupp, 1988; Zotov et al., 1995) but was found negligible in acidic solutions at $\geqslant$300 °C, in agreement with previous conclusions (Zotov et al., 2003).

The selection, among the Sb species from reactions 4 to 9, of the complexes formed in our experimental solutions in equilibrium with Sb_2O_3 or Sb_2S_3 was performed using the computer code HCh based on a free-energy minimization algorithm (Shvarov and Bastrakov, 1999). The Gibbs free energies of one or several Sb–OH–Cl complexes were adjusted in order to match both the measured solubilities at each NaCl–HCl composition point (reported in Tables 4–6) and the EXAFS-derived numbers of O and Cl ligands in the 2.3 m NaCl–0.1 m HCl solution in equilibrium with senarmontite. Note that the formation of hydroxy-chloride species via substitution of OH^- by Cl^- in the $Sb(OH)_3$ complex is strongly pH-dependent (reactions 5–9). Consequently, in most high-temperature runs where Sb dissolved concentrations were comparable to the HCl initial contents, values of pH in equilibrium with Sb_2O_3 and Sb_2S_3 cannot be estimated *a priori* from the initial HCl–NaCl solution composition because they strongly depend on the choice of dominant (hydroxy)chloride complexes. Consequently, only measured bulk solubilities together with independent information on O and Cl average coordination numbers in Experiments 2 and 3–4 (Table 3) were used as selection criteria. In these calculations, the thermodynamic properties of H_2O, H^+, OH^-, Na^+ and Cl^- were adopted from the SUPCRT92 database (Johnson et al., 1992); those for NaCl°, HCl° from Sverjensky et al. (1997) and Tagirov et al. (1997), respectively; and those for $Sb(OH)_3^\circ$, H_2S°, valentinite, senarmontite and stibnite were taken from Zotov et al. (2003). Both senarmontite and stibnite solubilities in pure water measured by XAFS and batch-reactor techniques in our study are in excellent agreement, within better than 0.05 log unit, with those predicted using the thermodynamic properties of the components cited above (Figs. 6 and 7). This supports the self-consistency of the thermodynamic data in the system Sb_2O_3–Sb_2S_3–H_2O reported by Zotov et al. (2003).

In NaCl–HCl solutions at 350 and 400 °C in equilibrium with senarmontite and stibnite, respectively, three species, $Sb(OH)_3^\circ$, $Sb(OH)_2Cl$° and $Sb(OH)_3Cl^-$, were found to reproduce the measured Sb_2O_3 and Sb_2S_3 solubilities within less than 0.1 log unit of total Sb concentration (Fig. 7). In addition, in a 2.3 m NaCl–0.1 m HCl solution in equilibrium with Sb_2O_3, the amounts of these three complexes calculated using their obtained formation constants correspond to average Cl and O coordination numbers of 0.6–0.4 and 2.2–2.4, respectively. This is in agreement with the EXAFS-derived values, assuming that the outer-sphere Cl atom in the $Sb(OH)_3Cl^-$ species is not seen by EXAFS (see Section 3.2).

In NaCl–HCl solutions at 300 °C in equilibrium with stibnite, it was found that the 3-species set adopted above matches the measured Sb contents at low HCl initial concentrations ($m_{HCl} \leqslant 0.03$, pH $\geqslant$ 2), but underestimates the experimental solubilities by more than 0.3 log unit at higher HCl concentrations ($0.1 \leqslant m_{HCl} \leqslant 0.2$, $1.5 \leqslant$ pH $\leqslant$ 2). This indicates the presence at strongly acid pH of complexes having more pronounced pH-dependences (e.g., reactions 6–9). Inclusion of either a pair of neutral

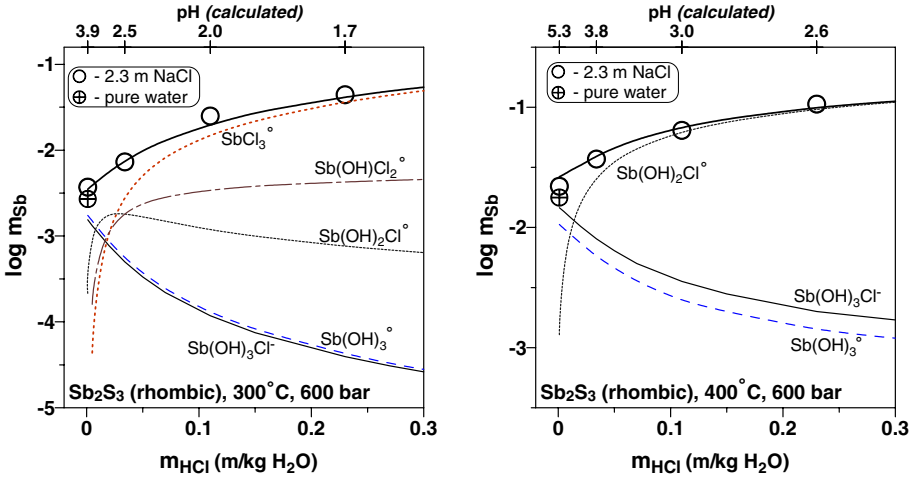

Fig. 7. Solubility of stibnite (Sb_2S_3, rhomb.) in a 2.3 m NaCl aqueous solution as a function of HCl concentration at 300 and 400 °C and 600 bar (see Table 6). Symbols represent experimental points obtained in this study from batch-reactor measurements; uncertainties on individual data points do not exceed the symbol size. Curves show total Sb concentration (solid-thick line) and amounts of each species in solution calculated in equilibrium with stibnite using the stability constants for Sb hydroxy-chloride species reported in Table 7 and the thermodynamic properties of Sb_2S_3 and $Sb(OH)_3^\circ$(aq) from Zotov et al. (2003).

species $Sb(OH)Cl_2^\circ$ and $SbCl_3^\circ$, or a single charged species, either $SbCl_2^+$ or $Sb(OH)Cl^+$, matched the experimental Sb_2S_3 solubilities at $m_{HCl} \geqslant 0.1$ m within better than 0.1 log unit (Fig. 7). It was, however, impossible to make a choice amongst these complexes because of the limited number of our solubility and XAFS data at low pH. All three groups of species whose stability was derived from the Sb_2S_3 solubility runs yielded similar average Cl and O numbers around Sb for the 2.3 m NaCl–0.1 m HCl–Sb_2O_3 system, $N_{Cl} \sim 0.6$–0.8 and $N_O \sim 2.0$–2.2, which is comparable within errors to the EXAFS-derived values at 300 °C (Table 3). Dissolved Sb concentrations predicted in equilibrium with Sb_2O_3 at 300 °C in this system are also similar, within ~30% of the value, to those measured in XAFS experiments. Because of the low sensitivity of stibnite solubility to different sets of species, we made a tentative choice of $Sb(OH)Cl_2^\circ$ and $SbCl_3^\circ$ as the dominant species in strongly acid solutions. This choice is corroborated by (i) the stepwise character of ion-exchange complexation reactions in solution; (ii) Sb(III) coordination chemistry which is characterized by tri-coordinated pyramidal geometries in Cl- and O-bearing solids (e.g., Svensson, 1974; Lipka, 1979) and solution (this study); (iii) the reluctance of Sb(III) to form charged species in moderately acid solutions; and (iv) the general tendency to favoring the formation of neutral species in high-temperature fluids. However, the formation of other species at high HCl and NaCl concentrations and moderate temperatures (<300 °C) cannot be completely excluded, and more experiments are needed to resolve this issue.

4.3. Stability constants of Sb(III) hydroxy-chloride species

The equilibrium reaction constants of formation of $Sb(OH)_3Cl^-$, $Sb(OH)_2Cl^\circ$, $Sb(OH)Cl_2^\circ$ and $SbCl_3^\circ$ according to Eqs. (4)–(7) are reported in Table 7. The two last complexes represent one of the possible choices for strongly acid solutions at 300 °C (see above); they are reported for consistency. At temperatures ⩾300 °C, the presence of these species was not detected at pH ⩾ 2.5, likely because of the significant decrease of both solution acidity and amount of free Cl^- ligand in HCl–NaCl solutions at such elevated temperatures, which should disfavor the stability of species with large Cl-ligand numbers. It is thus expected that $Sb(OH)_2Cl^\circ$ and $Sb(OH)_3Cl^-$ dominate, together with $Sb(OH)_3^\circ$, in slightly acidic to neutral natural fluids in a wide temperature range, and that the contribution of other (oxy)chloride species would be limited to very low pH (pH < ~2).

The stability constants of the two principal hydroxy-chloride complexes derived in this study at 300, 350 and 400 °C are plotted versus reciprocal temperature in Fig. 8. The formation constant of $Sb(OH)_2Cl^\circ$ (reaction 5) increases with increasing temperature, implying a positive enthalpy of the Cl–OH exchange reaction. This is in line with the analogous reaction of a hydroxy-fluoride complex formation, $Sb(OH)_2F^\circ$ (Popova et al., 1975). In contrast, the formation of the outer sphere $Sb(OH)_3Cl^-$ via reaction (4) is independent of temperature within errors, implying reaction enthalpy close to zero. This reaction energetics likely reflects non-specific charge-dipole interactions between the Cl^- anion and neutral $Sb(OH)_3^\circ$, characterized by large Sb–Cl distance and disorder, which may explain the non-detection of the Cl atom in this complex by EXAFS spectroscopy.

Assuming a linear dependence of log K versus $1/T$ which is typical of isocoulombic reactions, the equilibrium constants of reactions (4) and (5) can be extrapolated outside the 300-400 °C range using equations reported in Table 7. Calculations, using the predicted constant values, of the

Table 7
Stability constants for Sb(III) hydroxide and (hydroxy)-chloride aqueous complexes derived in this study from XAFS and batch-reactor solubility measurements

Reaction	T (°C)	P (bar)	Log_{10} K	Comments
$0.5Sb_2O_3$ (rhomb.) $+ 1.5H_2O = Sb(OH)_3^\circ$	60	Sat	-3.70 ± 0.05	Valentinite solubility in $NaClO_4$–$HClO_4$ solutions (see Electronic Annex)
	90	Sat	-3.32 ± 0.05	
$0.5Sb_2O_3$ (cub.) $+ 1.5H_2O = Sb(OH)_3^\circ$	250	600	-2.0 ± 0.1	XAFS
	300	600	-1.7 ± 0.1	XAFS
	350	300	-1.3 ± 0.1	Batch-reactor
	350	600	-1.35 ± 0.05	XAFS
	400	600	-1.08 ± 0.05	XAFS and batch-reactor
$Sb(OH)_3^\circ + H^+ = Sb(OH)_2^+ + H_2O$ [a]	60	Sat	0.83 ± 0.05	Valentinite solubility in $NaClO_4$–$HClO_4$ solutions (see Electronic Annex)
	90	Sat	0.7 ± 0.1	
$Sb(OH)_3^\circ + Cl^- = Sb(OH)_3Cl^-$ [b]	300	600	-0.2 ± 0.2	XAFS and batch-reactor solubility of senarmontite and stibnite
	350	600	0.0 ± 0.2	
	400	600	-0.1 ± 0.2	
$Sb(OH)_3^\circ + Cl^- = Sb(OH)_2Cl^\circ + OH^-$ [c]	300	600	-7.5 ± 0.5	XAFS and batch-reactor solubility of senarmontite and stibnite
	350	600	-7.1 ± 0.4	
	400	600	-6.2 ± 0.4	
$Sb(OH)_3^\circ + 2Cl^- = Sb(OH)Cl_2^\circ + 2OH^-$	300	600	-15.5 ± 1.0	Batch-reactor solubility of stibnite (tentative stoichiometry)
$Sb(OH)_3^\circ + 3Cl^- = SbCl_3^\circ + 3OH^-$	300	600	-23.1 ± 0.5	Batch-reactor solubility of stibnite (tentative stoichiometry)

[a] Log $K_{P_{sat}} = 800.1/T(K) - 1.5$, obtained from regression of valentinite solubility measurements at 60 and 90 °C from this study and literature data at 25 °C (see Electronic Annex).
[b] Log $K_{600b} = -519.4/T(K) + 0.8$, obtained from regression of data at 300, 350 and 400 °C from this study.
[c] Log $K_{600b} = -5000.5/T(K) + 1.1$, obtained from regression of data at 300, 350 and 400 °C from this study.

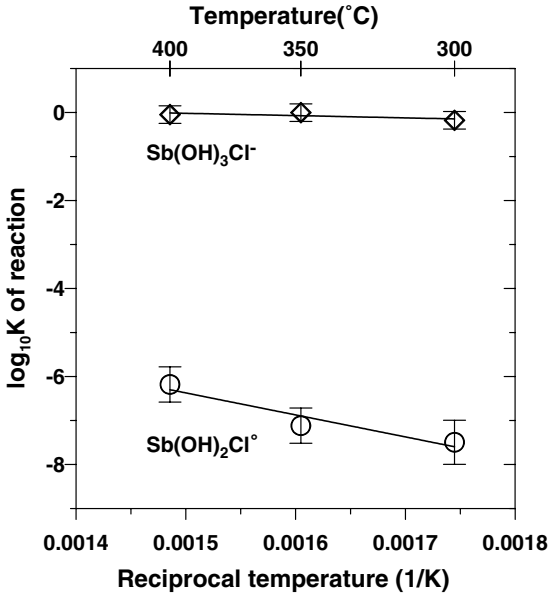

Fig. 8. Logarithms of the formation constants of $Sb(OH)_3Cl^-$ (diamonds) and $Sb(OH)_2Cl^\circ$ (circles) according to reactions (4) and (5) as a function of the reciprocal of absolute temperature at 600 bar. Symbols denote the data obtained in this study; lines represent their linear regression according to equations from Table 7.

amounts of total dissolved antimony and $Sb(OH)_3^\circ$, $Sb(OH)_2Cl^\circ$ and $Sb(OH)_3Cl^-$ in the system Sb_2O_3–2.3 m NaCl–0.1 m HCl compare favorably with the EXAFS-derived solubility and numbers of O and Cl ligands at 200, 250 and 450 °C. For example, at 450 °C/600 bar/$pH_{calc} \sim 4$, the predicted Sb_2O_3 solubility and average number of Cl ligands ($m_{Sb} = 0.29$, $N_{Cl} = 0.4$) are identical to the experimental values (Tables 3 and 4). At 200 °C/600 bar/$pH_{calc} \sim 1.3$, the calculated values ($m_{Sb} = 0.01$, $N_{Cl} = 0.3$) are also close to the experimental ones ($m_{Sb} = 0.009$, $N_{Cl} = 0.5$), even though they would be expected to underestimate the measurements because of the neglection of other Sb-chloride species at such low pH.

4.4. Computational uncertainties

The primary source of the uncertainties on the equilibrium constant values reported in Table 7 stems from those on experimental solubility and EXAFS coordination numbers and their regression using a chosen speciation scheme. Experimental uncertainties on XAFS and batch-reactor measured solubilities at each T–P-composition point are typically less than 0.1 log unit of total dissolved Sb concentration (Tables 4–6, Figs. 6, 7). The solubilities of Sb_2O_3 and Sb_2S_3 in pure water determined in this study are identical, within a similar error, to the previous work (Zotov et al., 2003). In addition, typical errors on the average number of neighbors around the Sb atom as determined by EXAFS and LCF regressions are ~10–20% and ~30% of the value for O and Cl, respectively (see Section 3.1 and Tables 1–3). This variation corresponds to an uncertainty of less than 0.1–0.2 log unit of concentration for the dominant $Sb(OH)_3^\circ$, $Sb(OH)_2Cl^\circ$ and $Sb(OH)_3Cl^-$ species in the system Sb_2O_3–2.3 m NaCl–0.1 m HCl for which

the Cl and O coordination numbers are available. Finally, regressions using the speciation scheme adopted in this study matched within ±0.1 log unit the entire set of Sb_2O_3 and Sb_2S_3 solubilities measured between 300 and 400 °C. Note however, that the error magnitudes in the calculated total solubility are roughly comparable to those for a given stability constant only if the corresponding species predominates in solution. Thus, the errors associated with the formation constant for $Sb(OH)_3Cl^-$ (reaction 4) which is dominant, together with $Sb(OH)_3^\circ$, at pH $\geqslant \sim 3$, are much smaller than those for $Sb(OH)_2Cl^\circ$ (reaction 5) which forms in comparable proportions with all other (oxy-)chloride species at pH $\leqslant 3$ (Fig. 9), so that large changes in its formation constant will affect only weakly the calculated total Sb solubility.

Another source of errors stem from the choice of thermodynamic data for major species in high-temperature concentrated NaCl–HCl solutions. In particular, because the H^+ (or OH^-) and Cl^- activities in solution largely control the extent of Sb–Cl complexation (reactions 4–9), they require good knowledge of NaCl° and HCl° stabilities. The dissociation constants of NaCl° (K_{NaCl}) adopted in this study are a result of regressions of many experimental data within the framework of the revised HKF equation of state (Sverjensky et al., 1997; references therein). The largest differences amongst the available data do not exceed ±0.2 of log K_{NaCl} values at the temperatures and pressures of this study. In addition, the results of the compilation of Sverjensky et al. (1997) are supported by the recent conductivity measurements of Ho et al. (1994) which yield K_{NaCl} values only ~0.2 log unit higher than those used in our study. This discrepancy corresponds to a difference of less than 10% for the concentrations of free Cl^- and Na^+ in a 2 molal NaCl solution between 300 and 400 °C, and thus has negligible effect on the stability constants for Sb hydroxy-chloride species. Triple ions like Na_2Cl^+ and $NaCl_2^-$ or bigger clusters may also form in NaCl solutions at temperatures above ~400 °C (Oelkers and Helgeson, 1990, 1993). Despite large errors likely associated with their degree of formation, their effect on the Sb–OH–Cl stability constants is expected to be similar to that of the NaCl° ion pair. The dissociation constants of HCl° (K_{HCl}) adopted in our study were taken from Tagirov et al. (1997) who compiled a large set of available data complemented by AgCl solubility measurements. The scatter between different data sets attains at least ±0.2–0.4 log K_{HCl} at our $T-P$ conditions, which would result in similar errors for calculated pH and $Sb(OH)_2Cl^\circ$ formation constant, and larger uncertainties for complexes with more pronounced pH dependence, like $Sb(OH)Cl_2^\circ$ and $SbCl_3^\circ$.

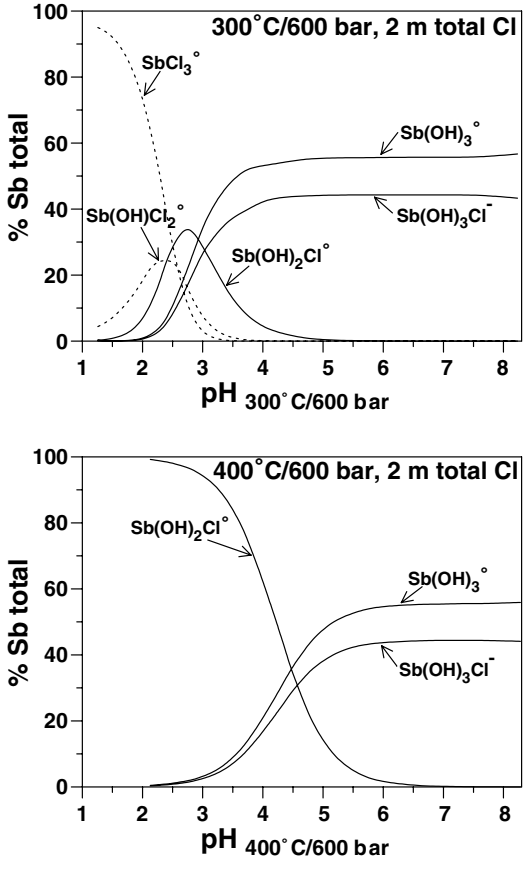

Fig. 9. Distribution of Sb(III) species in 2 m total Cl aqueous fluid as a function of pH at 300 °C/600 bar and 400 °C/600 bar, calculated using the stability constants reported in Table 7.

The third potential source of uncertainties may arise from the activity coefficients for neutral species such as Sb complexes, H_2S°, and HCl° in concentrated NaCl solutions at high temperatures. Although no data exist at present for activities of $Sb(OH)_3^\circ$ in NaCl solutions, by analogy with silicic acid, $Si(OH)_4^\circ$, it may be expected that Sb neutral complexes would exhibit "salting-in" behavior in high-temperature NaCl solutions, with negative values of the Setchenov coefficient (b_i, see Section 4.1). This would result in an increase of Sb_2O_3 solubility in NaCl fluids as it was observed for quartz (e.g., Xie and Walther, 1993). Thus, the slight disagreement between the number of Cl atoms around Sb seen by EXAFS (~0.4) and that which stems from the differences in solubilities of Sb_2O_3 in pure water and the 2.3 m NaCl–0.1 m HCl solution (~0.6–0.8, see Section 3.2) might, at least partially, be attributed to salting-in effects for $Sb(OH)_3^\circ$ resulting in enhanced oxide solubilities above 300 °C. However, it is difficult to predict the pressure and temperature dependence of the magnitude of such effects. For example, quartz solubility exhibits a ~2-fold increase at 400 °C and 500 bar in a 2 m NaCl solution in comparison to pure water ($b_{Si} \sim -0.3$), but this effect disappears almost completely with increasing pressure and decreasing temperature (e.g., $b_{Si} \sim 0$ at 400 °C/1000 bar and 300 °C/500–1000 bar, Xie and Walther, 1993). Assuming a similar effect for Sb_2O_3 would lower the stability of $Sb(OH)_3Cl^-$ by a factor of two at ~400 °C and ~600 bar. Thus, the increase of senarmontite solubility at slightly acid to neutral pH owing to salting-in effects for $Sb(OH)_3^\circ$ might be comparable to the magnitude of the outer-sphere $Sb(OH)_3Cl^-$ complex formation proposed in this study. Note, however, that the strong

solubility increase in more acid solutions cannot be explained solely by activity coefficients of neutral species. In contrast to non-volatile hydroxide complexes, volatile species like $H_2S°$, $HCl°$ and $SbCl_3^\circ$ usually exhibit a salting-out behavior in electrolyte solutions resulting in positive values of b_i, which yields activity coefficients above unity. This may significantly affect the interpretation of Sb_2S_3 solubilities at high NaCl concentrations. Unfortunately, the $P-T$ dependence of such effects remains poorly quantified. For example, values of b_{H_2S} in NaCl solutions at 300 °C and P_{sat} ($b_{H_2S} \sim 0.18$, Suleimenov and Krupp, 1994) decrease rapidly with increasing pressure but increase with increasing temperature at constant pressure ($b_{H_2S} \sim 0.04$ at 300 °C/400 bar; $b_{H_2S} \sim 0.50$ at 400 °C/400 bar, Ding and Seyfried, 1990). Although these scarce data do not allow accurate extrapolation to the higher pressures of our experiments, the use, in a rough approximation, of the b_{H_2S} values from Ding and Seyfried (1990) would increase the stability constants for oxy-chloride Sb species reported in Table 7 by 0.2–0.4 log units.

4.5. Comparison with previous work

To our knowledge, this is the first report of mixed hydroxy-chloride species of antimony in high-temperature geological fluids. Very little information exists on Sb–Cl interactions in saline solutions at elevated temperatures; most of it is based on the work of Ovchinnikov et al. (1982) who measured stibnite solubilities between 170 and 300 °C at saturated vapor pressure (P_{sat}) in NaCl–HCl solutions similar of those used in our study. The authors interpreted their data using Sb^{3+}, $Sb(OH)_3^\circ$ and a number of chloride species $SbCl_n^{3-n}$ ($1 \leqslant n \leqslant 4$); they concluded that Sb^{3+}, $SbCl_3^\circ$ and $SbCl_4^-$ dominate the Sb aqueous speciation at $pH \leqslant 3$ and $m_{NaCl} \geqslant 0.1$ between 200 and 300 °C. Their speciation scheme is, however, incompatible both with our EXAFS data on similar solutions, and Sb^{3+} hydrolysis which is characterized by the dominant formation of hydroxide species, $Sb(OH)_3$ and $Sb(OH)_2^+$ even at pH as low as 1 (this study; Popova et al., 1975; Baes and Mesmer, 1976; Zotov et al., 2003). In addition, their measured Sb_2S_3 solubilities are by a factor of 2–5 higher than those in our study at 300 °C. Regressions of the Ovchinnikov et al. (1982) solubility data with the set of species adopted in the present study resulted in a reasonable match of the measured values (±0.1 log unit) with $Sb(OH)_2Cl°$ and $Sb(OH)_3Cl^-$ dominant at moderately acid pH. However, the resulting stability constants at P_{sat} (~80 bar) were 1–2 orders of magnitude higher than those derived in our study at 600 bar. This disagreement is unlikely to result from pressure differences between their and our work, because no consistent pressure dependence of Sb_2S_3 solubility was found by our measurements (Table 6) or predicted by thermodynamic calculations (Zotov et al., 2003). Thus, these discrepancies might stem from poorly controlled H_2S partitioning into the vapor phase in the Ovchinnikov et al. (1982) experiments carried out at saturated vapor pressure which would result in an overestimation of Sb_2S_3 solubilities.

Our data indicate that the formation of the $Sb(OH)_3Cl^-$ species at neutral pH should increase Sb_2S_3 solubilities in NaCl solutions by a factor of 2–3 at $m_{NaCl} > 2$ m in comparison to pure water. This is in apparent disagreement with Wood et al. (1987) who measured solubilities of a mixture of metal sulfides (Sb_2S_3, ZnS, PbS, Ag_2S and Bi_2S_3) in the presence of the pyrite–pyrrhotite–magnetite assemblage (PyPoMt) in near-neutral 0–5 m NaCl solutions from 200 to 350 °C and pressures slightly above P_{sat}. Average stibnite solubilities reported in their work remain constant or slightly decrease with increasing NaCl content. However, the significant scatter (~ ± 1 log unit) of the reported data at NaCl concentrations above 2 m, and possibly incomplete H_2S buffering by the PyPoMt assemblage at the moderate temperatures of their study could mask the relatively small contribution from the Sb hydroxy-chloride complexes at neutral pH. At NaCl concentrations lower than 2 m, the uncertainties associated with the $Sb(OH)_3Cl^-$ stability constant (Table 7) are comparable to the amplitude of the predicted solubility increase thus further masking the effect of Sb hydroxy-chloride species on Sb minerals solubility in such systems.

5. Role of hydroxy-chloride complexes in antimony transport by hydrothermal fluids

Using the stability constants derived in our study, we calculated in Fig. 9 the distribution of Sb hydroxide and chloride complexes at 300 and 400 °C at 600 bar as a function of pH for a typical hydrothermal solution containing 10 ppm of Sb and 2 m of total chloride. It can be seen that at moderate temperatures (⩽300 °C) and acid pH (⩽3), Sb(III) speciation is represented by complexes $Sb(OH)_{3-n}Cl_n$ with $1 \leqslant n \leqslant 3$, and at higher pH by $Sb(OH)_3$ and $Sb(OH)_3Cl^-$ existing in comparable amounts. At higher temperatures, the single $Sb(OH)_2Cl°$ complex likely becomes the predominant species in acidic fluids ($pH \leqslant 4$); it is replaced by $Sb(OH)_3$ and $Sb(OH)_3Cl^-$ in slightly acid to neutral fluids whose pH is usually buffered by silicate mineral assemblages in high-temperature hydrothermal–magmatic systems. At such conditions, formation of the mixed oxy-chloride species is predicted to increase Sb-bearing mineral solubilities by a factor of 2–5 in the presence of significant amounts of salt (10–50 wt% NaCl) typical for fluids from porphyry-type deposits (e.g., Heinrich et al., 1999). At temperatures above 350 °C, the stabilities of these species imply Sb concentrations of thousands of ppm in order to saturate the fluid with stibnite, the principal Sb-bearing mineral in hypogene deposits. Considering the much lower concentrations of Sb found in natural hydrothermal fluids (<10–100 ppm), it is unlikely that Sb transport be controlled by solid-phase precipitation in high-temperature saline solutions. This may explain the scarcity of Sb-bearing minerals in deposits formed at temperatures above

350 °C (Williams-Jones and Normand, 1997). Because of the elevated solubilities of Sb hydroxide and hydroxy-chloride species at high temperature, the incorporation of significant amounts of Sb through isomorphic substitution in other sulfide minerals like pyrite or chalcopyrite is also unlikely. This is reflected by low Sb concentrations usually found in iron sulfides from magmatic–hydrothermal deposits. In contrast, with decreasing temperature, stibnite solubility drops very fast to concentrations as low as 1–10 ppm at 200–250 °C. Such solubilities are consistent with the typical conditions of stibnite precipitation in most Sb-bearing deposits (150–300 °C, Williams-Jones and Normand, 1997). Our calculations indicate that Sb hydroxy-chloride species are minor in the neutral solutions typical of Sb deposits formation, and that Sb speciation in such low- to moderate-temperature fluids is dominated by $Sb(OH)_3$ and eventually Sb-sulfide species.

In the absence of stable solid phases for Sb in high-temperature saline fluids, boiling and vapor-brine separation commonly observed in magmatic–hydrothermal deposits (e.g., Heinrich et al., 1999) may exert important control on Sb transport and distribution. Vapor phase is known to be more acid and enriched in volatile HCl than the dense brine as show experiments on brine–silicate–vapor systems (e.g., Shinohara and Fujimoto, 1994; Frank et al., 1998). Because antimony chloride and hydroxy-chloride species are more volatile than $Sb(OH)_3^\circ$ (e.g., Pokrovski et al., 2005b), they are expected to preferentially partition into the vapor phase. This is confirmed by the recent vapor–liquid fractionation measurements which show low values for Sb vapor–liquid partition coefficients, largely in favor of the NaCl-rich liquid at neutral pH ($K_{Sb} = [m_{Sb}$ in vapor$]/[m_{Sb}$ in liquid]; $K_{Sb} \sim 0.01$–0.001 at 350–450 °C). At acid pH ($m_{HCl} \sim 0.01$–0.1), the values of K_{Sb} increase by a factor of 10–100 due to the formation of volatile $SbCl_3$ and probably other hydroxy-chloride species (Pokrovski et al., 2005b). Thus, the elevated acidities which may occur in some high-temperature brine–vapor systems of porphyry environments will favor the formation of volatile Sb hydroxy-chloride species and thus significantly enhance Sb transfers by the ascending mobile vapor phase towards epithermal settings. In contrast, other metals like As, Zn, Cu, Ag and Au, do not exhibit significant changes in their vapor–liquid fractionation patterns in the H_2O–NaCl–HCl system as a function of HCl (Pokrovski et al., 2005b). Consequently, the vapor–liquid fractionation patterns for Sb which are very sensitive to pH and Cl contents may be indicative of the acidity conditions operating in magmatic–hydrothermal systems. For example, the elevated vapor–liquid partition coefficients for Sb, recorded in the coexisting vapor and brine fluid inclusions in some porphyry deposits from Romania and Argentinian Andes (e.g., Pettke et al., 2001), are likely due to formation of (hydroxy-)chloride species, and they may reflect high-acidity conditions in the boiling ore-forming hydrothermal fluid.

6. Concluding remarks

Solubility of senarmontite in $H_2O \pm NaCl \pm HCl$ solutions and local atomic structure around antimony(III) in the fluid were characterized by in situ X-ray absorption fine structure (XAFS) spectroscopy to 450 °C and 600 bar in a single series of measurements. Results show that Sb forms the neutral hydroxide species, $Sb(OH)_3$, in pure water; chloride complexes in concentrated HCl solutions; and mixed Sb–OH–Cl species in NaCl–HCl solutions typical of acidic high-temperature hydrothermal fluids.

These XAFS results combined with series of batch-reactor solubility measurements of senarmontite and stibnite as a function of NaCl and HCl contents in solution allowed quantification of the stabilities of the major Sb hydroxy-chloride species, $Sb(OH)_2Cl^\circ$ and $Sb(OH)_3Cl^-$, reported for the first time in the present study.

Thermodynamic calculations using the formation constants of Sb–OH–Cl complexes derived in this study indicate that these species, together with $Sb(OH)_3^\circ$, dominate Sb speciation in acidic to neutral chloride-rich high-temperature fluids ($\geqslant$300–350 °C) and lead both to enhanced Sb-bearing mineral solubilities and Sb partitioning into the vapor phase during vapor–brine separation processes at acidic conditions in magmatic-hydrothermal systems. However, these species remain minor in the neutral low- to moderate-temperature solutions ($\leqslant$250–300 °C) typical of Sb deposits formation, and the antimony speciation in such fluids is dominated by $Sb(OH)_3$ and eventually Sb-sulfide species.

This study demonstrated that XAFS spectroscopy can be used for direct and simultaneous in situ measurement of both solubilities and local atomic structure of metals in high-temperature geological fluids. Work is currently in progress to extend such measurements to solid–vapor and liquid–vapor partitioning for Sb and other metals (e.g., As, Au, Ag and Cu) over magmatic-hydrothermal conditions.

Acknowledgments

This work was supported by a CNRS grant from the French GDR program Transmet. We are grateful to the ESRF and French CRG Committees for providing beam time and access to the synchrotron facility. We are indebted to Gloria Subias Peruga, Olivier Proux and Vivian Nassif for their assistance during XAFS measurements at BM29 and BM30B beamlines, Olivier Geaymond for his help in the X-ray cell installation, Jean-Claude Harrichoury for his permanent support during solubility experiments, and Olivier Rouer and Alexandre Zotov for kindly supplying senarmontite and stibnite samples. Bruce Ravel is thanked for his advice on the Athena and Artemis software. Pierre Pokrovski (Pierrouchon) is acknowledged for his assistance in the manuscript preparation. Eric Oelkers and Mikhail Lemeshko are acknowledged for insightful discussions and suggestions. Editorial handling of the

Associate Editor Dimitri Sverjensky and constructive comments of two anonymous reviewers are greatly appreciated.

Associate editor: Dimitri A. Sverjensky

Appendix A. Supplementary data

Supplementary data associated with this article can be found, in the online version, at doi:10.1016/j.gca.2006.06.1549.

References

Abraitis, P.K., Pattrick, R.A.D., Vaughan, D.J., 2004. Variations in the compositional, textural and electrical properties of natural pyrite: a review. *Int. J. Miner. Process.* **74**, 41–59.

Allen, P.W., Sutton, L.E., 1950. Tables of interatomic distances and molecular configurations obtained by electron diffraction in the gas phase. *Acta Cryst.* **3**, 46–72.

Anderko, A., Pitzer, K.S., 1993. Equation-of-state representation of phase equilibria and volumetric properties of the system NaCl–H_2O above 573 K. *Geochim. Cosmochim. Acta* **57**, 1657–1680.

Ashley, P.M., Craw, D., Graham, B.P., Chappell, D.A., 2003. Environmental mobility of antimony around mesothermal stibnite deposits, New South Wales, Australia and southern New Zealand. *J. Geochem. Explor.* **77**, 1–14.

Audédat, A., Günther, D., Heinrich, C.A., 2000. Causes for large-scale metal zonation around mineralized plutons: fluid inclusion LA-ICP-MS evidence from the mole granite, Australia. *Econ. Geol.* **95**, 1563–1581.

Baes Jr., C.F., Mesmer, R.E., 1976. *The Hydrolysis of Cations*. Wiley, New York.

Bakker, R.J., 2003. Package FLUIDS 1. Computer programs for analysis of fluid inclusion data and for modelling bulk fluid properties. *Chem. Geol.* **194**, 3–23.

Belevantsev, V.I., Gushchina, L.I., Obolenskii, A.A., 1998. Antimony in hydrothermal solutions: analysis and generation of data on antimony(III) chloride species. *Geochem. Int.* **36**, 928–933.

Boyle, R.W., Jonasson, I.R., 1984. The geochemistry of antimony and its use as an indicator element in geochemical prospecting. *J. Geochem. Explor.* **20**, 223–302.

Brown Jr., G.E., Sturchio, N.C., 2002. An overview of synchrotron radiation applications to low temperature geochemistry and environmental sciences. *Rev. Miner. Geochim.* **49**, 1–115.

Chantler, C.T., Olsen, K., Dragoset, R.A., Kishore, A.R., Kotochigova, S.A., Zucker, D.S., 2003. X-ray form factor, attenuation and scattering tables (version 2.0). Available from <http://physics.nist.gov/ffast>. National Institute of Standards and Technology, Gaithersburg, MD.

Collings, M.D., Sherman, D.M., Ragnarsdottir, V.K., 2000. Complexation of Cu^{2+} in oxidized NaCl brines from 25 to 175 °C: results from in situ EXAFS spectroscopy. *Chem. Geol.* **167**, 65–73.

Cook, N.J., 1996. Mineralogy of the sulphide deposits at Sulitjelma, northern Norway. *Ore Geol. Rev.* **11**, 303–338.

Crerar, D., Wood, S., Brantley, S., 1985. Chemical controls on solubility of ore-forming minerals in hydrothermal solutions. *Can. Miner.* **23**, 333–352.

Cromer, D.T., Liberman, D., 1970. Relativistic calculations of anomalous scattering factors for X-rays. *J. Chem. Phys.* **53**, 1891–1898.

Crozier, E.D., Rehr, J.J., Ingalls, R., 1988. Amorphous and liquid systems. In: Koningsberger, D.C., Prins, R. (Eds.), *X-Ray Absorption: Principles, Applications, Techniques of EXAFS, SEXAFS and XANES*. Wiley-Interscience, New York, pp. 373–442.

Ding, K., Seyfried, W.E., 1990. Activity coefficients of H_2, H_2S in NaCl solutions at 300–425 °C, 300–500 bars with application to ridge crest hydrothermal systems. *EOS* **71** (43), 1680.

Filella, M., Belzile, N., Chen, Y.-W., 2002. Antimony in the environment: a review focused on natural waters I. Occurrence. *Earth Sci. Rev.* **57**, 125–176.

Filella, M., May, P.M., 2003. Computer simulation of the low-molecular-weight inorganic species distribution of antimony(III) and antimony(V) in natural waters. *Geochim. Cosmochim. Acta* **67**, 1013–1031.

Filipponi, A., Borowski, M., Bowron, D.T., Ansell, S., De Panfilis, S., Di Cicco, A., Itie, J.-P., 2000. An experimental station for advanced research on condensed matter under extreme conditions at the European synchrotron radiation facility-BM29 beamline. *Rev. Sci. Instrum.* **71**, 2422–2432.

Frank, M.R., Candela, P.A., Piccoli, P.M., 1998. K–feldspar–muscovite–andalusite–quartz–brine phase equilibria: an experimental study at 25 to 60 MPa and 400 to 550 °C. *Geochim. Cosmochim. Acta* **62**, 3717–3727.

Heinrich, C.A., Günther, D., Audédat, A., Ulrich, T., Frischknecht, R., 1999. Metal fractionation between magmatic brine and vapour, and the link between porphyry-style and epithermal Cu–Au deposits. *Geology* **27**, 755–758.

Helgeson, H.C., Kirkham, D.H., 1974. Theoretical prediction of the thermodynamic behavior of aqueous electrolytes at high pressures and temperatures: II. Debye–Hückel parameters for activity coefficients and relative partial molal properties. *Am. J. Sci.* **274**, 1199–1261.

Ho, P.C., Palmer, D.A., Mesmer, R.E., 1994. Electrical conductivity measurements of aqueous sodium chloride solutions to 600 °C and 300 MPa. *J. Sol. Chem.* **23**, 997–1018.

Johnson, J.W., Oelkers, E.H., Helgeson, H.C., 1992. SUPCRT92: a software package for calculating the standard molal thermodynamic properties of minerals, gases, aqueous species, and reactions from 1 to 5000 bar and 0 to 1000 °C. *Comput. Geosci.* **18**, 899–947.

Kestin, J., Sengers, J.V., Kamgar-Parsi, B., Levelt Sengers, J.M.H., 1984. Thermophysical properties of fluid H_2O. *J. Phys. Chem. Ref. Data* **13**, 175–183.

Krupp, R.E., 1988. Solubility of stibnite in hydrogen sulfide solutions, speciation, and equilibrium constants, from 25 to 350 °C. *Geochim. Cosmochim. Acta* **52**, 3005–3015.

Lipka, A., 1979. An X-ray structure determination of antimony trichloride. *Acta Cryst.* **B35**, 3020–3022.

Marshall, W.L., Chen, C-T.A., 1982. Amorphous silica solubilities-IV. Postulated sulfate–silicic acid complex. *Geochim. Cosmochim. Acta* **46**, 367–370.

Mayanovic, R.A., Anderson, A.J., Bassett, W.A., Chou, I.M., 2001. Hydrogen bond breaking in aqueous solutions near the critical point. *Chem. Phys. Lett.* **336**, 212–218.

Mernagh, T.P., Heinrich, C.A., Leckie, J.F., Carville, D.P., Gilbert, D.J., Valenta, R.K., Wyborn, L.A.I., 1994. Chemistry of low-temperature hydrothermal gold, platinum, and palladium (±uranium) mineralization at Coronation Hill, Northern Territory, Australia. *Econ. Geol.* **89**, 1053–1073.

Milne, J., 1975. Spectrophotometric studies on Sb(III) in hydrochloric acid solutions. *Can. J. Chem.* **53**, 888–893.

Newville, M., Livins, P., Yacoby, Y., Stern, E.A., Rehr, J.J., 1993. Near-edge X-ray-absorption fine structure of Pb: a comparison of theory and experiment. *Phys. Rev.* **B47**, 14126–14131.

Newville, M., 2001. IFEFFIT: interactive XAFS analysis and FEFF fitting. *J. Synchrotron Radiat.* **8**, 322–324.

Oelkers, E.H., Helgeson, H.C., 1990. Triple-ion anions and polynuclear complexing in supercritical electrolyte solutions. *Geochim. Cosmochim. Acta* **54**, 727–738.

Oelkers, E.H., Helgeson, H.C., 1993. Calculation of dissociation constants and the relative stabilities of polynuclear clusters of 1:1 electrolytes in hydrothermal solutions at supercritical pressures and temperatures. *Geochim. Cosmochim. Acta* **57**, 2673–2697.

Oelkers, E.H., Sherman, D.M., Ragnarstottir, K.V., Collins, C., 1998. An EXAFS spectroscopic study of aqueous antimony(III)-chloride complexation at temperatures from 25 to 250 °C. *Chem. Geol.* **151**, 21–27.

Ovchinnikov, L.N., Kozlov, Y.D., Rafal'sky, R.P., 1982. The solubility of stibnite in chloride solutions at elevated temperatures. *Geochem. Int.* **19** (5), 56–63.

Pauling, L., 1948. *The Nature of the Chemical Bond*. Cornell University Press, Ithaca, NY.

Perfetti, E., 2003. Mesures expérimentales volumiques et calorimétriques de arsenic (III) et (V) en solution à 25–350 °C et 0.1–29 MPa. Applications aux systèmes naturels. *Master's Thesis*, University Blaise Pascal, Clermont-Ferrand, France (in French).

Pettke, T., Halther, W.E., Driesner, T., von Quadt, A., Heinrich, C.A., 2001. The porphyry to epithermal link: preliminary fluid chemical results from the Apuseni Mountains, Romania, and Famatina, Argentinian Andes. *11th Annual V.M. Goldschidt Conference, Journal of Conference Abstracts,* 3537.pdf.

Pokrovski, G.S., Kara, S., Roux, J., 2002a. Stability and solubility of arsenopyrite, FeAsS, in crustal fluids. *Geochim. Cosmochim. Acta* **66**, 2361–2378.

Pokrovski, G.S., Zakirov, I.V., Roux, J., Testemale, D., Hazemann, J.L., Bychkov, A.Y., Golikova, G.V., 2002b. Experimental study of arsenic speciation in vapor phase to 500 °C: Implications for As transport and fractionation in low-density crustal fluids and volcanic gases. *Geochim. Cosmochim. Acta* **66**, 3453–3480.

Pokrovski, G.S., Roux, J., Hazemann, J.L., Testemale, D., 2005a. An X-ray absorption spectroscopy study of argutite solubility and germanium aqueous speciation in hydrothermal fluids to 500 °C and 400 bar. *Chem. Geol.* **217**, 127–145.

Pokrovski, G.S., Roux, J., Harrichoury, J.C., 2005b. Fluid density control on vapor–liquid partitioning of metals in hydrothermal systems. *Geology* **33**, 657–660.

Popova, M.Y., Khodakovsky, I.L., Ozerova, N.A., 1975. Experimental determination of the thermodynamic properties of antimony hydroxide and hydroxy-fluoride complexes at temperatures to 200 °C. *Geokhimia* **6**, 835–843 (in Russian).

Proux, O., Biquard, X., Lahera, E., Menthonnex, J.-J., Prat, A., Ulrich, O., Soldo, Y., Trevisson, P., Kapoujyan, G., Perroux, G., Taunier, P., Grand, D., Jeantet, P., Deleglise, M., Roux, J.-P., Hazemann, J-L., 2005. FAME: a new beamline for X-ray absorption investigations of very diluted systems of environmental, material and biological interests. *Phys. Scripta* **T115**, 970–973.

Proux, O., Nassif, V., Prat, A., Ulrich, O., Lahera, E., Biquard, X., Menthonnex, J.-J., Hazemann, J.-L., 2006. Feedback system of a liquid-nitrogen-cooled double-crystal monochromator: design and performances. *J. Synchrotron Radiat.* **13**, 59–68.

Ravel, B., Newville, M., 2005. ATHENA, ARTEMIS, HEPHAESTUS: data analysis for X-ray absorption spectroscopy using IFEFFIT. *J. Synchrotron Radiat.* **12**, 537–541.

Rouxel, O., Ludden, J., Fouquet, Y., 2003. Antimony isotope variations in natural systems and implications for their use as geochemical tracers. *Chem. Geol.* **200**, 25–40.

Rudnick, R.L., Gao, S., 2003. Composition of the continental crust. In: Holland, H.D., Turekian, K.K. (Eds.), *Treatise on Geochemistry*. Elsevier, Amsterdam.

Seward, T.M., Henderson, C.M.B., Charnock, J.M., 2000. Indium(III) chloride complexing and salvation in hydrothermal solutions to 350 °C: an EXAFS study. *Chem. Geol.* **167**, 117–127.

Sherman, D.M., 2001. Quantum chemistry and classical simulations of metal complexes in aqueous solutions. *Rev. Miner. Geochem.* **42**, 273–317.

Shinohara, H., Fujimoto, K., 1994. Experimental study in the system albite–andalusite-quartz–NaCl–HCl–H_2O at 600 °C and 400 to 2000 bars. *Geochim. Cosmochim. Acta* **58**, 4857–4866.

Shock, E.L., Oelkers, E.H., Johnson, J.W., Sverjensky, D.A., Helgeson, H.C., 1992. Calculation of the thermodynamic properties of aqueous species at high pressures and temperatures: effective ionic radii, dissociation constants, and standard partial molal properties to 1000 °C and 5 kbar. *J. Chem. Soc. Faraday Trans.* **88**, 803–826.

Shvarov, Y.V., Bastrakov, E., 1999. *HCh: a software package for geochemical equilibrium modelling*. User's Guide. Australian Geological Survey Organization, record 1999/25.

Simmons, S.F., Browne, P.R.L., 2000. Hydrothermal minerals and precious metals in the Braodlands–Ohaaki geothermal system: Implications for understanding low-sulfidation epithermal environments. *Econ. Geol.* **95**, 971–999.

Simonet, V., Calzavara, Y., Hazemann, J-L., Argoud, R., Geaymond, O., Raoux, D., 2002. X-ray absorption spectroscopy of ionic association in aqueous solutions of zinc bromide from normal to critical conditions. *J. Chem. Phys.* **117**, 2771–2781.

Spycher, N.F., Reed, M.H., 1989. As(III) and Sb(III) sulfide complexes: an evaluation of stoichiometry and stability from existing experimental data. *Geochim. Cosmochim. Acta* **53**, 2185–2194.

Suleimenov, O.M., Krupp, R.E., 1994. Solubility of hydrogen sulfide in pure water and in NaCl solutions, from 20 to 320 °C and at saturation pressures. *Geochim. Cosmochim. Acta* **58**, 2433–2444.

Svensson, C., 1974. The crystal structure of orthorhombic antimony trioxide, Sb_2O_3. *Acta Cryst.* **B30**, 458–461.

Sverjensky, D.A., Shock, E.L., Helgeson, H.C., 1997. Prediction of the thermodynamic properties of aqueous metal complexes to 1000 °C and 5 kb. *Geochim. Cosmochim. Acta* **61**, 1359–1412.

Tagirov, B.R., Zotov, A.V., Akinfiev, N.N., 1997. Experimental study of the dissociation of HCl from 350 to 500 °C and from 500 to 2500 bar. Thermodynamic properties of HCl°(aq). *Geochim. Cosmochim. Acta* **61**, 4267–4280.

Tanger, J.C., Helgeson, H.C., 1988. Calculation of the thermodynamic and transport properties of aqueous species at high pressures and temperatures: revised equations of state for the standard partial molal properties of ions and electrolytes. *Am. J. Sci.* **288**, 19–98.

Testemale, D., Hazemann, JL., Pokrovski, G.S., Joly, Y., Roux, J., Argoud, R., Geaymond, O., 2004. Structural and electronic evolution of As(III) atomic environment in hydrothermal solutions: an EXAFS and XANES investigation. *J. Phys. Chem.* **121**, 8973–8982.

Testemale, D., Argoud, R., Geaymond, O., Hazemann, J-L., 2005. High pressure/high temperature cell for X-ray absorption and scattering techniques. *Rev. Sci. Instrum.* **76**, 043905–043909.

Williams-Jones, A.E., Normand, C., 1997. Controls of mineral parageneses in the system Fe–Sb–S–O. *Econ. Geol.* **92**, 308–324.

Wilson, N.J., Craw, D., Hunter, K., 2004. Antimony distribution and environmental mobility at an historic antimony smelter site, New Zealand. *Environ. Pollut.* **129**, 257–266.

Wood, S., 1989. Raman spectroscopic determination of ore metals in hydrothermal solutions: I. Speciation of antimony in alkaline sulfide solutions at 25 °C. *Geochim. Cosmochim. Acta* **53**, 237–244.

Wood, S., Crerar, D.A., Borcsik, M.P., 1987. Solubility of the assemblage pyrite–pyrrhotite–magnetite–sphalerite–galena–gold–stibnite–bismuthinite–argentite–molybdenite in H_2O–NaCl–CO_2 solutions from 200 to 350 °C. *Econ. Geol.* **82**, 1864–1887.

Xie, Z., Walther, J.V., 1993. Quartz solubilities in NaCl solutions with and without wollastonite at elevated temperatures and pressures. *Geochim. Cosmochim. Acta* **57**, 1947–1955.

Zabinsky, S.I., Rehr, J.J., Ankudinov, A.L., Albers, R.C., Eller, M.J., 1995. Multiple-scattering calculations of X-ray-absorption spectra. *Phys. Rev.* **B52**, 2995–3009.

Zaytsev, I.D., Aseyev, G.G., 1985. *Properties of Aqueous Solutions of Electrolytes*. CRC Press, Boca Raton.

Zotov, A.V., Kudrin, A.V., Levin, K.A., Shikina, N.D., Varyash, L.N., 1995. Experimental studies of the solubility and complexing of selected ore elements (Au, Ag, Cu, Mo, As, Sb, Hg) in aqueous solutions. In: Shmulovich, K.I., Yardley, B.W.D., Gonchar, G.G. (Eds.), *Fluids in the Crust: Equilibrium and Transport Properties*. Chapman and Hall, pp. 95–137.

Zotov, A.V., Shikina, N.D., Akinfiev, N.N., 2003. Thermodynamic properties of the Sb(III) hydroxide complex $Sb(OH)_3$(aq) at hydrothermal conditions. *Geochim. Cosmochim. Acta* **67**, 1821–1836.

Zotov, N., Keppler, H., 2002. Silica speciation in aqueous fluids at high pressures and temperatures. *Chem. Geol.* **184**, 71–82.